Acta Mech
https://doi.org/10.1007/s00707-023-03531-4

ORIGINAL PAPER

Kazuhiro Oda · **Takayuki Shinmoto** · **Nao-Aki Noda**

Thermal stress intensity factor of an edge interface crack under arbitrary material combination considering double singular stress fields before and after cracking

Received: 25 October 2022 / Revised: 14 February 2023 / Accepted: 19 February 2023

Abstract This paper discusses the stress intensity factor (SIF) for an edge interfacial crack in a wide bimaterial plate under uniform temperature change. The results shows that the SIF is controlled by the singular stress field including a constant term appearing at the interface end of the bimaterial plate without the crack. Since the constant term peculiar to thermal loading is necessary to be considered, it is confirmed that the SIF is analyzed by superposing the SIF under tension and the SIF under uniform interface stress. Finally, the SIF under thermal stress is systematically calculated and tabulated for arbitrary material combination in the whole range of Dundurs parameters α and β. When $\alpha = 2\beta$, the SIF is presented as a function of α ($= 2\beta$) by considering the logarithmic-type edge singularity, which is also peculiar to the thermal loading.

List of symbols

SIF	Stress intensity factor
ISSF	Intensity of singular stress field
FEM	Finite element method
K_σ, k_σ	Intensity of singular stress field (ISSF)
K_1, K_2	Stress intensity factors (SIF) for interface crack in target problem
$K_1{}^*$, $K_2{}^*$	Stress intensity factors (SIF) for interface crack in reference problem
F_1, F_2	Dimensionless SIF
C_1, C_2, D_1, D_2	Dimensionless coefficients of SIF
c_1, c_2, d_1, d_2	Dimensionless coefficients of SIF
ΔT	Uniform temperature change
$\sigma_y(r)$, $\tau_{xy}(r)$	Normal or shearing stress along the interface
G_A, G_B	Shear modulus of material A, B
ν_A, ν_B	Poisson's ratio of material A, B
η_A, η_B	Thermal expansion coefficient of material A, B

K. Oda
Division of Mechanical Engineering, Faculty of Science and Technology, Oita University, 700 Dannoharu, Oita-Shi, Oita 870-1192, Japan
e-mail: oda-kazuhiro@oita-u.ac.jp

T. Shinmoto
Mechanical and Energy Systems Engineering Course, Graduate School of Oita University, 700 Dannoharu, Oita-Shi, Oita 870-1192, Japan

N.-A. Noda (✉)
Department of Mechanical Engineering, Kyushu Institute of Technology, 1-1 Sensui-Cho, Tobata-Ku, Kitakyushu-Shi, Fukuoka 804-8550, Japan
e-mail: nao592noda@gmail.com

Published online: 31 March 2023

α, β	Dundurs composite parameters
λ	Singularity index at interface end
ε	Oscillation singular index for interface crack
a	Interface crack length
W	Plate width
T, S	Tensile and shear stresses in reference problem
$\sigma_{y0,\mathrm{FEM}}$, $\tau_{xy0,\mathrm{FEM}}$	Crack tip stress calculated by FEM in unknown problem under uniform temperature change
$\sigma^{*}_{y0,\mathrm{FEM}}$, $\tau^{*}_{xy0,\mathrm{FEM}}$	Crack tip stress calculated by FEM in reference problem under the remote stresses T and S
$\sigma^{T=1*}_{y0,\mathrm{FEM}}$, $\tau^{T=1*}_{xy0,\mathrm{FEM}}$	Crack tip stress calculated by FEM in reference problem under the tensile stress $T = 1$ ($S = 0$)
$\sigma^{S=1*}_{y0,\mathrm{FEM}}$, $\tau^{S=1*}_{xy0,\mathrm{FEM}}$	Crack tip stress calculated by FEM in reference problem under the shear stress $S = 1$ ($T = 0$)
σ_{y0}	Equivalent stress in y-direction when $\alpha(\alpha - 2\beta) > 0$
σ_{x0}	Equivalent stress in x-direction when $\alpha(\alpha - 2\beta) = 0$

1 Introduction

In recent years, electronic components such as semiconductors have become highly integrated, and thermal stress caused by the different expansion coefficient becomes more problematic. Furthermore, the temperature change in automobiles, computers, etc. in a day increases greatly causing many mechanical failures such as reduced strength at the joint interface due to thermal stress, cracking of constituent materials and delamination at the interface of dissimilar materials. Several previous studies have considered the singular stress field at the interface end to evaluate such problems [1–6]. Since fracture of the bonding material often occurs from the interface end, the analysis of the edge interface crack is mandatory for evaluating the interface failure. To evaluate the stress intensity factor (SIF) of an edge interface crack, care should be taken for two distinct singular stress fields existing: One is caused by the bonded plate end before cracking and the other is due to the interface crack itself after cracking. Figure 1 illustrates the double singular stress fields whose SIF was clarified by applying the proportional method in the preceding papers [7, 8]. As shown in Sect. 3 and Appendix A, the proportional method may provide exact solutions. Then, the results showed that when the relative crack length $a/W \leq 10^{-2}$ (see Fig. 10), the SIF is dominated by the singular stress field in Fig. 1b [8]. Noda and Lan [8] presented a suitable form to express the stress intensity factor for arbitrary material combinations by taking into account the edge singularity.

However, the singular stress field under thermal loading has some differences compared to the one under tensile loading [3, 9, 10]. First, unlike under mechanical loading, a constant term existing around the interface end peculiar to thermal loading must be taken into account [9, 10]. Due to the constant term before cracking, the thermal SIF becomes more complex compared to mechanical loading. Therefore, to understand the double singular stress fields is more important especially for thermal loading. Second, no analytical thermal loading solution is available for interface edge crack under arbitrary material combinations except for the semi-infinitely long cracks [11, 12]. Third, certain specific material combinations may cause a logarithmic-type singular stress field unlike tensile loading where only a power function-type singular stress field appears [10].

Therefore, in this study, the SIF of the edge interface crack under uniform temperature change will be clarified in comparison with the one under tension. The SIF is controlled by the thermal stress generated when a uniform temperature change is applied. Since the SIF becomes larger especially when the crack length is smaller due to the singular stress before cracking, the problem of small edge crack will be focused. The small edge crack is essential because the SIFs of large edge cracks is quite small under thermal loading (see Table 10 in Appendix B). First, the difference of the singular stress field without crack will be clarified under mechanical and thermal loading. Then the SIF will be analyzed systematically by varying the material combination. Finally, the SIF will be newly provided under arbitrary material combinations. The proposed solution for the edge interface crack will be able to provide SIFs for arbitrary material combinations under mechanical and thermal loads without numerical calculations.

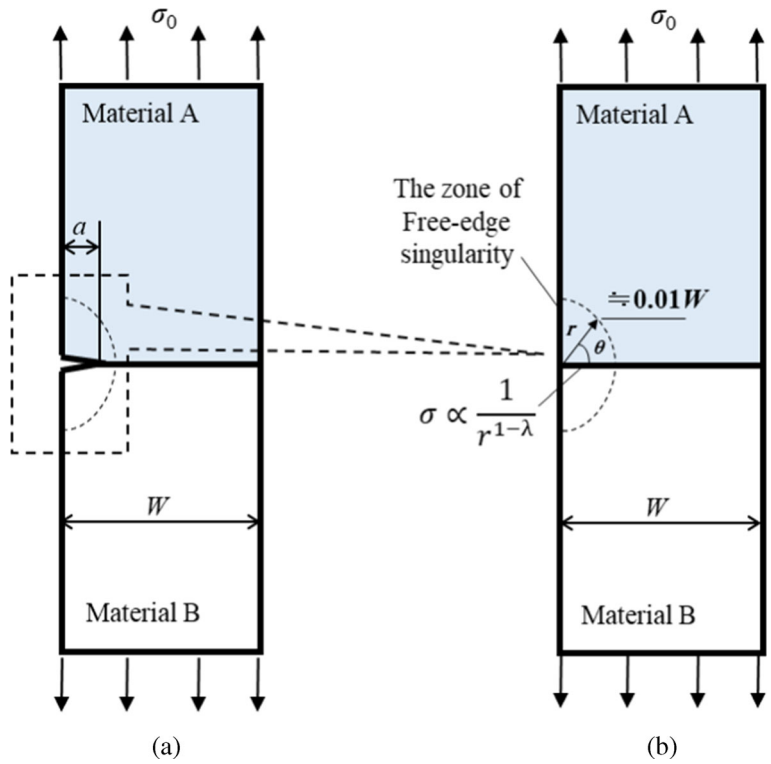

Fig. 1 Illustration of double singular stress fields: **a** The stress intensity factor (SIF) controlling the singular stress field of an edge interface crack in **a** is controlled by **b** the intensity of the singular stress field (ISSF) controlling the singular stress field of the bonded AB plate without crack in **b**

2 Difference of singular stress field of a bimaterial plate before cracking under tension and thermal loading

To understand the SIF of an edge interface crack under thermal loading, it is necessary to know the singular stress without crack since the double singularities in Fig. 1 must be considered. In the previous studies, Bogy pointed out the existence of logarithmic singularity in dissimilar bonded plates under surface traction without mentioning the equivalent tensile stress of the thermal loading [13]. Chen et al. [6] explained that the stress distribution due to thermal loading can be expressed by the stress distribution under tension and the constant uniform stress without mentioning that the meaning of the constant stress value. Therefore, in this Sect. 2, the interfacial stress distributions under tension and thermal loading will be indicated with the difference of the singular stress distribution. Then, the value of the constant stress will be clarified to understand the edge interface crack problem [6, 13].

2.1 Interface stress distribution under tension when $\boldsymbol{\alpha(\alpha - 2\beta) > 0}$

Figure 2a shows the stress distribution $\sigma_y(r)$ at the interface end due to the remote tensile stress $\sigma_y^{\infty}(x) = \sigma_0$ when $\alpha = 0.8$, $\beta = 0.3$. Without losing generality, the remote tensile stress can be put as $\sigma_y^{\infty}(x) = \sigma_{y0}$, which will be defined later in Eq. (6) as shown in Fig. 2a. The singular stress distribution near the interface edge $\sigma_y(r)$ can be expressed in Eq. (1).

$$\sigma_y(r) = \frac{K_\sigma}{r^{1-\lambda}} \tag{1}$$

Here, K_σ is the intensity of the singular stress field (ISSF) and λ is the edge singularity index whose value is given by the characteristic equation of Eq. (2) [14].

$$\left[\sin^2\left(\frac{\pi}{2}\lambda\right) - \lambda^2\right]^2\beta^2 + 2\lambda^2\left[\sin^2\left(\frac{\pi}{2}\lambda\right) - \lambda^2\right]\alpha\beta + \lambda^2(\lambda^2 - 1)\alpha^2 + \frac{\sin^2(\lambda\pi)}{4} = 0 \tag{2}$$

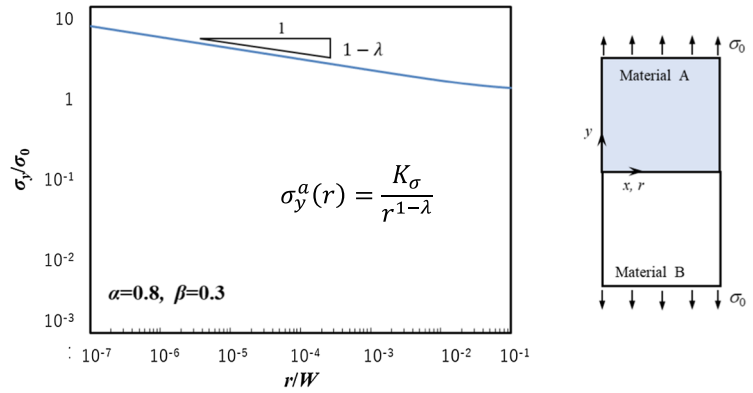

(a) Interface stress distribution $\sigma_y^a(r)$ due to remote tensile loading $\sigma_y^\infty(x) = \sigma_0$ when $\alpha = 0.8,\ \beta = 0.3$

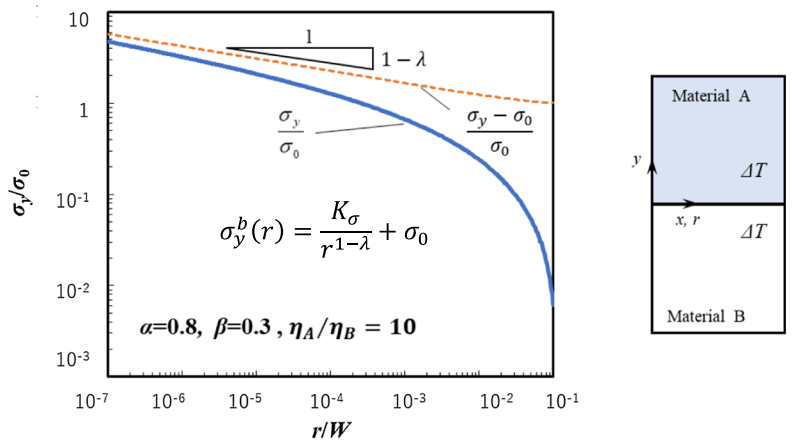

(b) Interface stress distribution $\sigma_y^b(r)$ due to negative uniform temperature change $\Delta T = T_0 < 0$ when $\alpha = 0.8,\ \beta = 0.3$

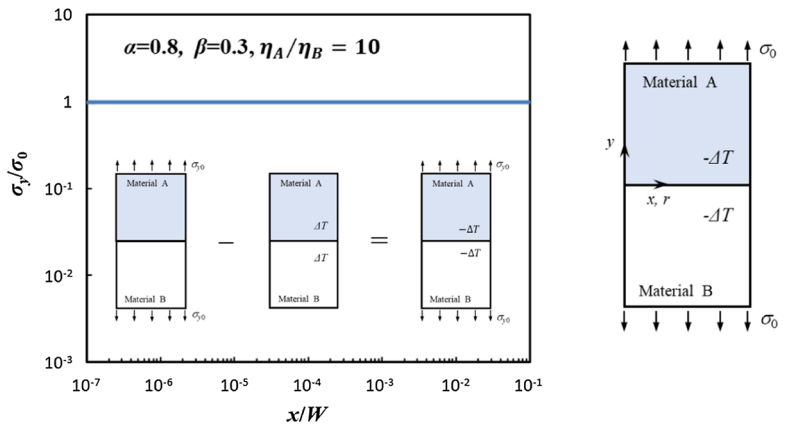

(c) Constant interface stress distribution $\sigma_y^c(r) = \sigma_0$ obtained by subtracting Fig.3 (b) from Fig.3 (a) as $\sigma_y^c(r) = \sigma_y^a(r) - \sigma_y^b(r) = \sigma_0$ when $\alpha = 0.8,\ \beta = 0.3$

Fig. 2 Interface stress distribution $\sigma_y(r)$ under mechanical loading and thermal loading. Those results are obtained when $\alpha = 0.8$, $\beta = 0.3$, ($G_A/G_B = 10.93$, $\nu_A/\nu_B = 0.0314$, plane stress), $\Delta T = T_0 = -100$ deg, thermal expansion coefficient ratio $\eta_A/\eta_B = 10$

Table 1 Behaviors of the interface stress $\sigma_y(r)$ when $r \to 0$ in Fig. 2 under mechanical loading and thermal loading

Material combination	Under thermal loading	Under mechanical loading
$\alpha(\alpha-2\beta) > 0$ (bad pair)	$\sigma_y(r) = \frac{K_\sigma}{r^{1-\lambda}} + \sigma_{y0} \to \infty (r \to 0)$	$\sigma_y(r) = \frac{K_\sigma}{r^{1-\lambda}} \to \infty (r \to 0)$
$\alpha(\alpha-2\beta) = 0$ (equal pair)	$\sigma_y(r) = k_\sigma \log(r) \to \infty (r \to 0)$ $(\alpha \neq 0)$	$\sigma_y(r) \to$ finite$(r \to 0)$
$\alpha(\alpha-2\beta) < 0$ (good pair)	$\sigma_y(r) \to$ finite$(r \to 0)$	$\sigma_y(r) \to 0 (r \to 0)$

In Eq. (2), Dundurs parameters α, β are determined from the material combination as follows [14].

$$\alpha = \frac{G_A(\kappa_B+1) - G_B(\kappa_A+1)}{G_A(\kappa_B+1) + G_B(\kappa_A+1)}, \beta = \frac{G_A(\kappa_B-1) - G_B(\kappa_A-1)}{G_A(\kappa_B+1) + G_B(\kappa_A+1)}, \tag{3}$$

$$\kappa_m = \begin{cases} (3-\nu_m)/(1+\nu_m) & \text{(plane stress)} \\ 3-4\nu_m & \text{(plane strain)} \end{cases} (m = A, B) \tag{4}$$

The singularity index $\lambda < 1$ obtained from Eq. (2) characterizes the presence of the singular stress in Fig. 1b in the following way.

(1) When $\alpha(\alpha-2\beta) > 0$ (bad pair), $0 < \lambda < 1$.
(2) When $\alpha(\alpha-2\beta) = 0$ (equal pair), $\lambda = 1$.
(3) When $\alpha(\alpha-2\beta) < 0$ (good pair), $\lambda > 1$.

Table 1 summarizes the characteristic of singular stress fields under mechanical loading in comparison within the case of thermal loading.

2.2 Interface stress distribution under thermal loading when $\boldsymbol{\alpha(\alpha-2\beta) > 0}$

The presence or absence of the interface stress singularity was discussed in the previous studies [6, 10]. Table 1 summarizes the behaviors of the interface stress $\sigma_y(r)$ when $r \to 0$ in Fig. 2 under mechanical loading and thermal loading. The interface stress behavior varies depending on $\alpha(\alpha-2\beta) > 0$, $\alpha(\alpha-2\beta) = 0$, $\alpha(\alpha-2\beta) < 0$.

Figure 2b shows the stress distribution $\sigma_y(r)$ at the interface edge due to the thermal loading by cooling the plate's temperature uniformly as $\Delta T = T_0 < 0$. Fig. 2b is an example when $\alpha = 0.8$, $\beta = 0.3$, $T_0 = -100$ deg and thermal expansion coefficient ratio $\eta_A/\eta_B = 10$. To conform the constant term peculiar to the thermal loading, Fig. 2c shows the subtracted distribution of Fig. 2b from Fig. 2a. As shown in Fig. 2c, a constant interface stress distribution $\sigma_y^c(r) = \sigma_{y0}$ is confirmed as can be expressed $\sigma_y^c(r) = \sigma_y^a(r) - \sigma_y^b(r) = \sigma_{y0}$. The dashed line in Fig. 2b is the stress σ_y at the interface due to the uniform temperature change $\Delta T = -T_0 < 0$ subtracting the constant term $\sigma_y = \sigma_{y0}$ in Fig. 2c.

From Fig. 2, it can be confirmed that the singular stress distribution under thermal loading in Fig. 2b at the interface end $\sigma_y(r)$ can be expressed in Eq. (5).

$$\sigma_y(r) = \frac{K_\sigma}{r^{1-\lambda}} + \sigma_{y0} \tag{5}$$

In other words, under the bad pair condition satisfying $\alpha(\alpha-2\beta) > 0$ the power function-type singular stress field $r^{1-\lambda}$ occurs in the case of the thermal load as well as in the case of the mechanical load causing $\sigma_y(r) \to \infty$ as $r \to 0$.

The constant term σ_{y0} is known as the equivalent remote tensile stress that should be applied to the bimaterial plate (see Fig. 2a) to produce the same ISSF (see Fig. 2b). Under the remote tensile stress σ_{y0} defined in Eq. (6), the same intensity of the singular stress K_σ due to the uniform temperature change $\Delta T = -T_0 < 0$ can be obtained [6].

$$\sigma_{y0} = \frac{8G_AG_B\left(\eta_B^* - \eta_A^*\right)\Delta T}{G_A(\kappa_B-1) - G_B(\kappa_A-1) - 2(G_A-G_B)},$$

$$\eta_m^* = \begin{cases} \eta_m & \text{(plane stress)} \\ (1+\nu_m)\,\eta_m & \text{(plane strain)} \end{cases} (m = A, B) \tag{6}$$

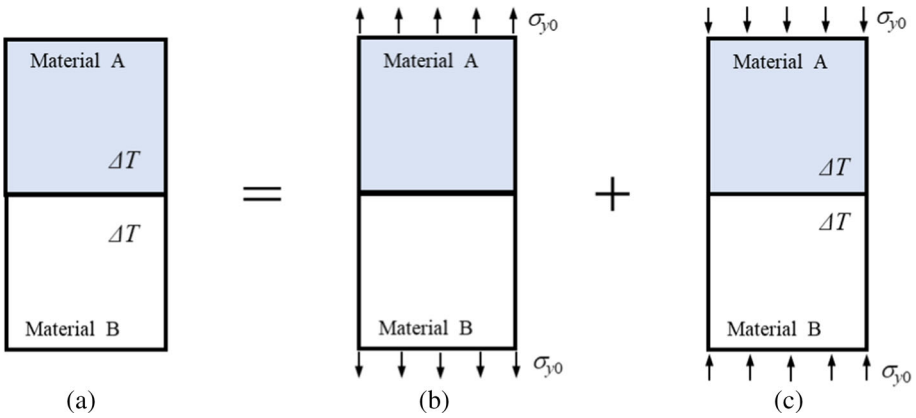

Fig. 3 **a** Singular interface stress due to uniform thermal loading $\Delta T = T_0 < 0$ can be expressed by superposing **b** tensile loading and **c** constant interface stress when $\alpha(\alpha - 2\beta) > 0$. The constant interface stress in **c** can be obtained from compressive σ_{y0} and $\Delta T = T_0 < 0$

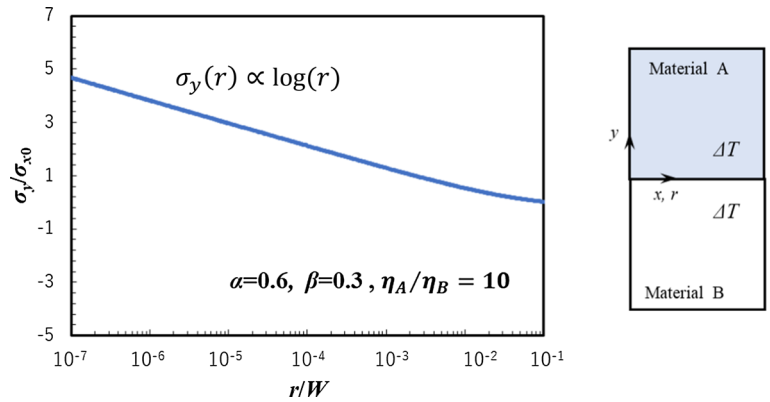

Fig. 4 Stress distribution near the interface edge in bimaterial plate when $\alpha - 2\beta = 0$, $\alpha = 0.6$, $\beta = 0.3$, $\Delta T = -100$ deg, thermal expansion coefficient ratio $\eta_A/\eta_B = 10$.

Here, G_A, G_B are shear modulus, ν_A, ν_B are Poisson's ratio and η_A^*, η_B^* are thermal expansion coefficient of material A, B, respectively.

Figure 3 illustrates the idea of the analysis method used later in Sect. 4. The stress distribution in Fig. 3a under thermal loading consists of the one under the tensile loading in Fig. 3b and the constant interface stress in Fig. 3c. The SIF solution in Fig. 3b was analyzed previously. As shown in Fig. 3c, the uniform interface stress in Fig. 3c is expressed by the sum of the compressive remote loading and the thermal loading. In this study, the stress intensity factor of the edge crack in the bimaterial plate under uniform temperature change will be discussed on the basis of the superposition in Fig. 3.

2.3 Interface stress distribution under thermal loading when $\boldsymbol{\alpha(\alpha - 2\beta) = 0}$

It is known that even when $\alpha(\alpha - 2\beta) = 0$, which is named equal pair condition under mechanical loading, a logarithmic singularity occurs for thermal loading [10]. In other words, under the equal pair condition $\alpha(\alpha - 2\beta) = 0$, $\sigma_y(r) \to$ finite as $r \to 0$ in the case of mechanical load, whereas in the case of thermal load, logarithmically singular stress field is generated and $\sigma_y(r) \to \infty$ when $r \to 0$. Figure 4 shows an example of logarithmic singular stress distribution under equal pair conditions, and $\sigma_y(r) \to \infty$ when $r \to 0$ when $\alpha = 0.6$, $\beta = 0.3$.

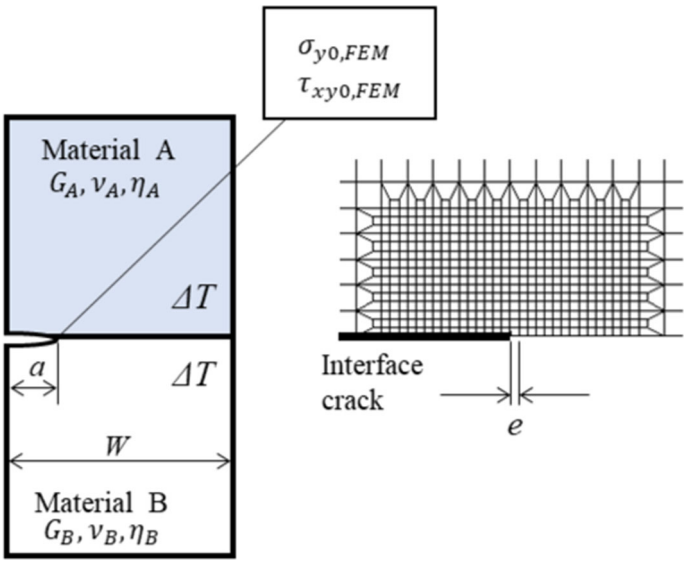

Fig. 5 Unknown problem for an edge interface crack in bimaterial rectangular plate subjected to uniform temperature change ΔT. The stress values at the crack tip $\sigma_{y0,FEM}$, $\tau_{xy0,FEM}$ are calculated by FEM considering the elastic modulus G_A, ν_A, G_B, ν_B and thermal expansion coefficients η_A, η_B

2.4 Interface stress distribution under thermal loading when $\boldsymbol{\alpha(\alpha - 2\beta) < 0}$

Under good pair condition $\alpha(\alpha - 2\beta) < 0$, the stress singularity disappears in the case of the thermal load as well as in the case of the mechanical load, and $\sigma_y(r) \to 0$ as $r \to 0$. In the case of $\alpha(\alpha - 2\beta) < 0$, no singular stress field occurs, so in this sense $\alpha(\alpha - 2\beta) < 0$ is a good pair even for thermal loading.

3 Analysis method of interfacial cracks under thermal load and influence of material combination

3.1 Proportional method to analyze thermal interface stress intensity factors

Figure 5 shows a bimaterial plate with an edge interface crack subjected to uniform temperature change ΔT, which is the target problem in this study. In the FEM analysis, a uniform temperature change ΔT is applied to the entire element in Fig. 5 considering elastic modulus and thermal expansion coefficient. Then, the stress value at the crack tip is calculated. In a similar way, an interface edge crack under heat flow may be solved after analyzing temperature distribution [19]. Since the singular field appears at the interface end of the bonded plate without crack, the discussion in Sect. 2 must be useful for heat flow problems. In this study, the SIF of the interface crack under uniform temperature change ΔT is focused by applying the proportional method [15–17]. As shown in the preceding papers as well as the following explanation in Sects. 3 and 4, the proportional method may provide exact solutions [7, 8, 15–17].

In the method, stress values at the crack tip node are used and a stress intensity factor is determined by the ratio of the crack tip stress values between an unknown problem in Fig. 5 and the reference problem in Fig. 6. The method gives the singular stress field equal to the unknown problem by adjusting load stress T and S of the reference problem whose stress intensity factor is already known. The single interface crack in a bonded semi-infinite plate subjected to the tension T and shear S is selected as the reference problem because the interface crack tip is always mixed mode state. The stress values at the interface crack tip node calculated by FEM in the reference problem under the tensile stress $T = 1$ ($S = 0$) or shear stress $S = 1$ ($T = 0$) are written by $\sigma_{y0,FEM}^{T=1*}$, $\tau_{xy0,FEM}^{T=1*}$ and $\sigma_{y0,FEM}^{S=1*}$, $\tau_{xy0,FEM}^{S=1*}$, respectively, in Fig. 6. The crack tip stress values of the unknown problem under the uniform temperature change in Fig. 5 are also denoted by $\sigma_{y0,FEM}$, $\tau_{xy0,FEM}$. By using the same crack tip stress condition between the reference and the unknown problems, that is, $\sigma_{y0,FEM} = \sigma_{y0,FEM}^{*}$ and $\tau_{xy0,FEM} = \tau_{xy0,FEM}^{*}$, the external loading stress T and S in the reference problem can be determined from the next expression.

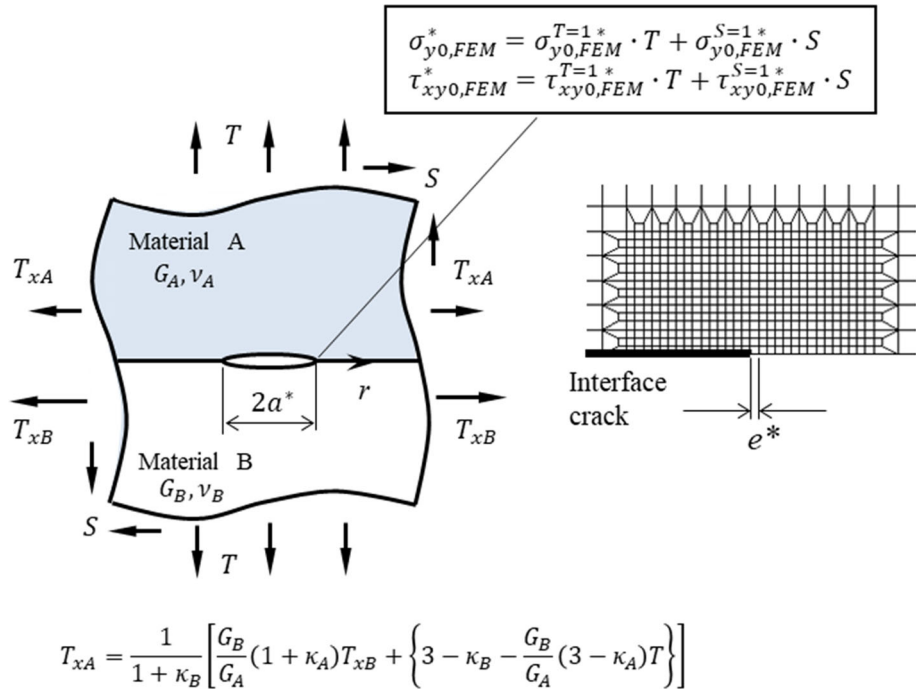

Fig. 6 Reference problem for an interface crack in a bonded semi-infinite plate subjected to tension T and shear S

$$
\begin{aligned}
T &= \frac{\sigma_{y0,\mathrm{FEM}} \cdot \tau^{S=1*}_{xy0,\mathrm{FEM}} - \sigma^{S=1*}_{y0,\mathrm{FEM}} \cdot \tau_{xy0,\mathrm{FEM}}}{\sigma^{T=1*}_{y0,\mathrm{FEM}} \cdot \tau^{S=1*}_{xy0,\mathrm{FEM}} - \sigma^{S=1*}_{y0,\mathrm{FEM}} \cdot \tau^{T=1*}_{xy0,\mathrm{FEM}}}, \\
S &= \frac{\sigma^{T=1*}_{y0,\mathrm{FEM}} \cdot \tau_{xy0,\mathrm{FEM}} - \sigma_{y0,\mathrm{FEM}} \cdot \tau^{T=1*}_{xy0,\mathrm{FEM}}}{\sigma^{T=1*}_{y0,\mathrm{FEM}} \cdot \tau^{S=1*}_{xy0,\mathrm{FEM}} - \sigma^{S=1*}_{y0,\mathrm{FEM}} \cdot \tau^{T=1*}_{xy0,\mathrm{FEM}}}
\end{aligned}
\tag{7}
$$

From the loading stresses T and S obtained by Eq.(7), the stress intensity factor of the interface crack in the reference problem in Fig.6 can be evaluated by

$$
K_1^* + iK_2^* = (T + iS)\sqrt{\pi a^*}(1 + 2i\varepsilon),\ \varepsilon = \frac{1}{2\pi}\ln\left[\left(\frac{\kappa_A}{G_A} + \frac{1}{G_B}\right)/\left(\frac{\kappa_B}{G_B} + \frac{1}{G_A}\right)\right] \tag{8}
$$

Here, ε is the oscillation singular index, $\kappa_m = 3 - 4\nu_m$(plane strain), $(3 - \nu_m)/(1 + \nu_m)$(plane stress). Because the stress intensity factor of Eq. (8) is equal to that of the unknown problem, the stress intensity factors of the unknown problem in Fig. 5 can be obtained as

$$
K_1 = K_1^*, \quad K_2 = K_2^* \tag{9}
$$

From $K_1 = K_1{}^*$, $K_2 = K_2{}^*$, (T, S) in Eq. (8) can be regarded as dimensionless SIFs (F_1, F_2) of unknown problem [see Eq. (11))]. It is noted that in the proportional method the finite element models of the reference and the unknown problems have the same crack length and the same FEM mesh pattern near the interface crack tip [7, 8, 15–17], $a = a^*$ and $e = e^*$. The definition of stress intensity factor shown in Eq. (8) is expressed as follows based on the interface crack length $2a^*$.

$$
\sigma_y(r) + i\tau_{xy}(r) = \frac{K_1 + i\ K_2}{\sqrt{2\pi r}}\left(\frac{r}{2a^*}\right)^{i\varepsilon} \tag{10}
$$

The detail of the accuracy discussion can be found in previous papers under mechanical loading [8, 15, 16]. The proportional method is useful for analyzing interface cracks by providing mesh-independent interface SIFs F_1, F_2 efficiently. Since those FEM results are mesh-independent, the obtained SIFs K_1, K_2 can be regarded as the exact solution by using the exact reference solution in the bonded infinite plate $K_1 + iK_2 = (T + iS)\sqrt{\pi a}(1 + 2i\varepsilon)$. For the readers' convenience, several examples are indicated in Appendix A.

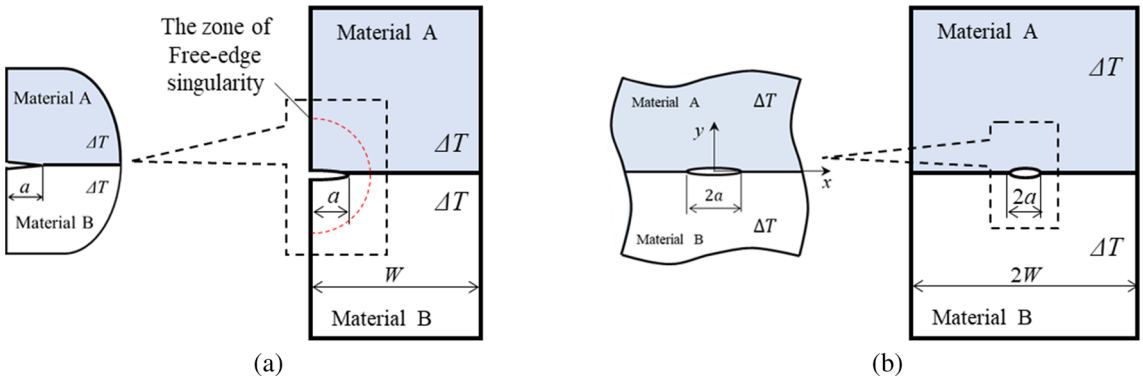

Fig. 7 Comparison between the edge interface crack and the central interface crack by taking an example of the bimaterial plate $\alpha = 0.8$, $\beta = 0.3$, $a/W = 10^{-5}$ subjected to uniform temperature change $\Delta T = T_0 = -100$ deg, thermal expansion coefficient ratio $\eta_A/\eta_B = 10$. Here, the constant term stress σ_{y0} is defined by Eq. (6)

3.2 Importance of edge interface crack under thermal loading compared to internal crack

Figure 7 shows an edge interface crack in a bimaterial plate considered in this paper in comparison with a central interface crack in a bimaterial plate. When $a/W \to 0$, those problems are reduced to most fundamental crack problems, that is, a cracked semi-infinite plate and a cracked infinite plate. For example, when the two materials have the same material properties, they correspond to an edge crack in a homogeneous semi-infinite plate and an internal crack in a homogeneous infinite plate. In this study, the dimensionless stress intensity factors F_1, F_2 defined in Eq. (11) will be compared by applying the proportional method in Sect. 3.1.

$$K_1 + iK_2 = (F_1 + iF_2)\sigma_{y0}\sqrt{\pi a}(1 + 2i\varepsilon) \tag{11}$$

The thermal stress intensity factors K_1, K_2 depend on the temperature change ΔT, Dunders parameter α, β, thermal expansion coefficient ratio η_A/η_B and relative crack length a/W. When uniform temperature change $\Delta T = T_0 = -100$ deg is applied to the cracked bimaterial plate with $\alpha = 0.8$, $\beta = 0.3$ and $a/W = 10^{-5}$, the dimensionless SIFs are obtained as $F_1 = 2.568$ and $F_2 = -0.364$ in Fig. 7a. Instead, in Fig. 7b, the dimensionless SIFs are obtained as $F_1 = -0.0214$ and $F_2 = 1.7 \times 10^{-5}$, whose values are much smaller than $F_1 = 2.568$ in Fig. 7a. Furthermore, when the tensile thermal stress appears at the interface end, the compressive thermal stress occurs at the center of the bimaterial plate. This is because the summation of σ_y along the interface is zero and only at the interface end the singular stress appears. In this way, it may be concluded that regarding thermal stress intensity factors the small edge interface crack is essential and practically important.

3.3 Effect of material combination on the thermal interface stress intensity factors

The thermal stress intensity factors K_1, K_2 depend on the temperature change ΔT, Dunders parameter α, β, thermal expansion coefficient ratio η_A/η_B and relative crack length a/W. Table 2 shows the values of F_1, F_2 of the edge interface crack by varying material constants but under fixed $\alpha = 0.8$, $\beta = 0.3$ with $a/W = 10^{-5}$. Table 2 shows that even if the material constants are different, the values of F_1, F_2 are the same. This is because Dundurs parameters α, β control F_1, F_2.

To clarify the effects of the crack length and the material combination, Fig. 8 shows F_1, F_2 by varying the crack length as $a/W = 10^{-7} \sim 10^{-1}$ by taking an example when $\alpha = 0.5 \sim 0.95$ and $\beta = 0.3$. When $\alpha = 0.5 \sim 0.55$ with $\beta = 0.3$, the good pair condition $\alpha(\alpha - 2\beta) < 0$ can be satisfied; then, the dimensionless SIF F_1, $F_2 \to$ finite as $a/W \to 0$. However, when $\alpha = 0.65 \sim 0.95$ with $\beta = 0.3$, the bad pair condition $\alpha(\alpha - 2\beta) > 0$ can be satisfied; then, F_1, $|F_2| \to \infty$ as $a/W \to 0$. This is due to the singular stress field at the interface end under the bad pair condition. Due to the singularity, as the crack becomes shorter as $a/W \to 0$, the stress at the crack tip goes to infinity. Figure 8, for the small interface crack, shows that the expression of F_1, F_2 in Eq. (11) is not enough and the double singular stress fields have to be considered. In Fig. 9, the equal pair condition $\alpha(\alpha - 2\beta) > 0$ is not considered, the equivalent stress $\sigma_{y0} \to \infty$. In Sect. 4, F_1, F_2 in Eq. (11) will be defined in a different way of Eq. (11).

Table 2 Confirmation of the thermal SIFs F_1, F_2 defined from $K_1 + iK_2 = (F_1 + iF_2)\sigma_{y0}\sqrt{\pi a}(1 + 2i\varepsilon)$ that are controlled by α, β by taking an example when $\alpha = 0.8$, $\beta = 0.3$ and $a/W = 10^{-5}$ in Fig. 5

Analysis conditions		Case 1 (Plane stress)	Case 2 (Plane stress)	Case 3 (Plane strain)	Case 4 (Plane strain)
Shear modulus [MPa]	G_A	496.524	4878.049	99.999	3998.612
	G_B	45.426	453.515	9.091	363.625
Poisson's ratio	ν_A	0.007	0.025	0.000011	0.000347
	ν_B	0.223	0.225	0.181819	0.181844
Thermal expansion [1/K]	η_A	10	10	5	3
	η_B	1	100	2	20
Temperature change [K]	ΔT	100	100	100	100
Equivalent stress (Eq. 6)	σ_{y0}	450,000	− 45,000,000	26,364	− 8,254,337
Normalized SIF	F_1	2.5675	2.5675	2.5675	2.5675
	F_2	− 0.3635	− 0.3635	− 0.3635	− 0.3635

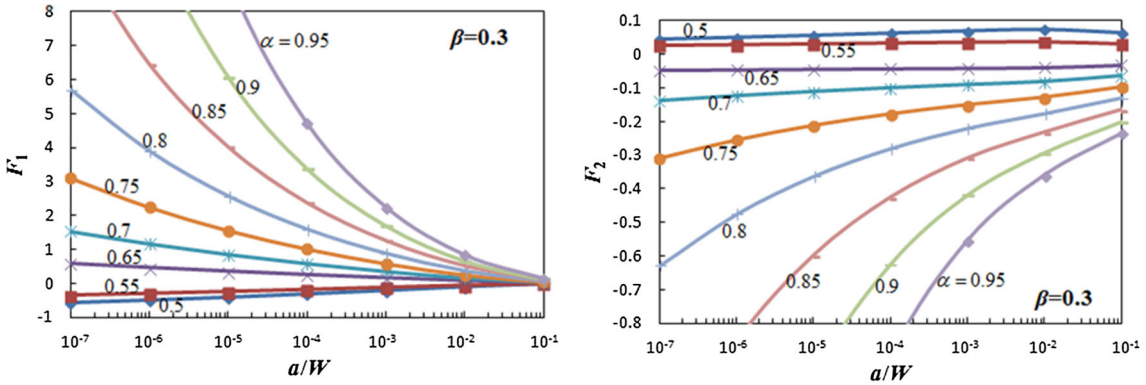

(a) (b)

Fig. 8 Relation between normalized SIFs F_1, F_2 and the relative crack length a/W when $\beta = 0.3$ in Fig. 7a, $[K_1 + iK_2 = (F_1 + iF_2)\sigma_{y0}\sqrt{\pi a}(1 + 2i\varepsilon)]$

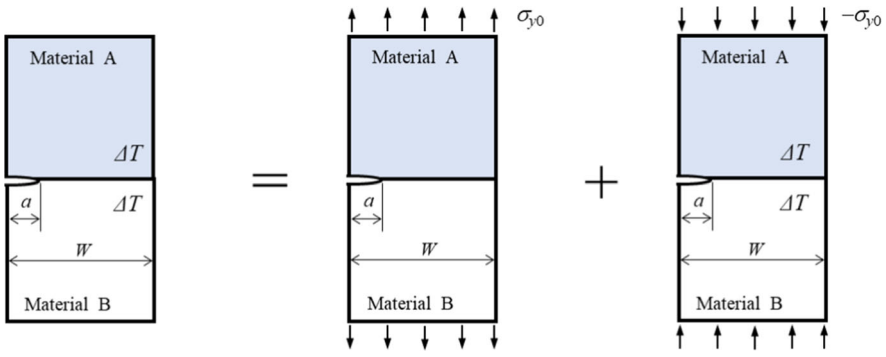

(a) $F_1 = C_1 \cdot (W/a)^{1-\lambda} + D_1$ (b) $F_1 = C_1 \cdot (W/a)^{1-\lambda}$ (c) $F_1 = D_1$

$F_2 = C_2 \cdot (W/a)^{1-\lambda} + D_2$ $F_2 = C_2 \cdot (W/a)^{1-\lambda}$ $F_2 = D_2$

Fig. 9 **a** Singular interface stress due to uniform thermal loading $\Delta T = T_0 < 0$ can be expressed by superposing **b** tensile loading and **c** constant interface stress when $\alpha(\alpha - 2\beta) > 0$. The constant interface stress in Fig. 10c can be obtained from compressive σ_{y0} and $\Delta T = T_0 < 0$

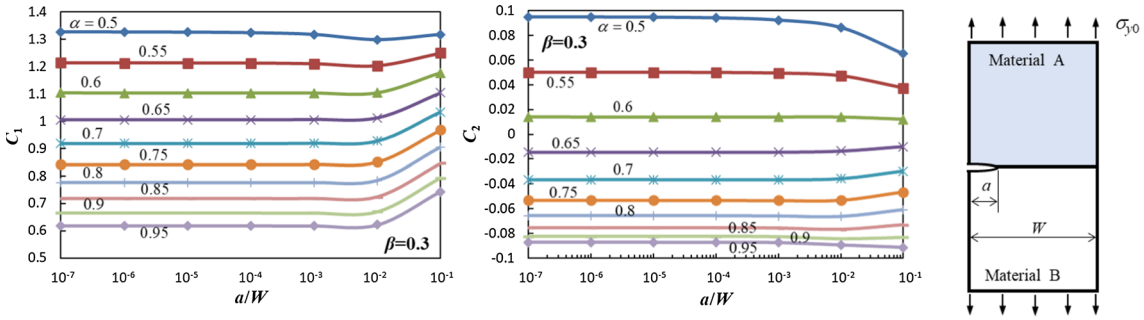

Fig. 10 Values of $C_1 = F_1/(W/a)^{1-\lambda}$ and $C_2 = F_2/(W/a)^{1-\lambda}$ in Fig. 9b by varying a/W in the range $a/W = 10^{-7}$~10^{-1} and also by varying α in the range $\alpha = 0.5 \sim 0.95$ under fixed β=0.3

Table 3 Behaviors of dimensionless SIFs F_1, F_2 when $a/W \to 0$ in Fig. 5 under mechanical loading and thermal loading corresponding to the behaviors of the interface stress $\sigma_y(r)$ in Table 1. [$K_1 + iK_2 = (F_1 + iF_2)\sigma_0\sqrt{\pi a}(1 + 2i\varepsilon)$, where σ_0 is the equivalent stress defined by Eq. (6) or Eq. (15)]

Material combination	Under thermal loading	Under mechanical loading
$\alpha(\alpha - 2\beta) > 0$ (bad pair)	$F_1, F_2 \to \infty\left(\frac{a}{W} \to 0\right)$	$F_1, F_2 \to \infty\,(a/W \to 0)$
$\alpha(\alpha - 2\beta)$=0 (equal pair)	$F_1, F_2 \to \infty(a/W \to 0)$ (logarithmic singularity when $\alpha \neq 0$)	$F_1, F_2 \to$ finite $(a/W \to 0)$
$\alpha(\alpha - 2\beta) < 0$ (good pair)	$F_1, F_2 \to$ finite$(a/W \to 0)$	$F_1, F_2 \to 0\,(a/W \to 0)$

Table 3 summarizes the behavior of SIFs under mechanical loading and thermal loading, that is, F_1, $F_2 \to \infty$, F_1, $F_2 \to$ finite or F_1, $F_2 \to 0$ as $a/W \to 0$ inFig. 5. Comparison between Table 1 and Table 3 shows that $\sigma_y(r)$ and F_1, F_2 have the same behavior; for example, when the singular stress field without crack exists as $\sigma_y(r) \to \infty$, F_1, $F_2 \to \infty$. In other words, the dimensionless SIFs F_1, F_2 are totally controlled by the interface stress $\sigma_y(r)$ without crack.

4 Stress intensity factor for interfacial edge crack in bimaterial plate based on the principle of superposition

4.1 Stress intensity factor of a small edge crack in bimaterial plate considering the edge singularity of the power function type

In this section, the SIF of a small interface crack in bimaterial plate in Fig. 9a will be analyzed on the basis of the discussion in Sect. 2. As shown in Fig. 9, the singular stress field at the edge of the interface in Fig. 9a due to the thermal loading can be expressed by superposing the tensile loading in Fig. 9b and the constant interface stress in Fig. 9c [6]. In Fig. 9, the uniform stress field at the interface in Fig. 9c is expressed by the sum of the compressive remote loading and the thermal loading.

To express the SIF of the edge interface crack under uniaxial tension in Fig. 9b, the coefficients C_1, C_2 were newly proposed as shown in Eq. (12) [8] considering the interface end singularity without crack. Then, the coefficients C_1, C_2 in Fig. 9b were obtained by the proportional method using FEM confirming more than three digits convergence.

$$K_1 + iK_2 = (F_1 + iF_2)\sigma_{y0}\sqrt{\pi a}(1 + 2i\varepsilon),\ F_1 = C_1 \cdot (W/a)^{1-\lambda},\ F_2 = C_2 \cdot (W/a)^{1-\lambda} \tag{12}$$

when α(α-2β) ≠ 0 in Fig. 9b

As shown in Fig.16 in Appendix B, as $a/W \to 0$, F_1, F_2 are not suitable for expressing the SIF sinceF_1 $\to \infty$, $F_2 \to \infty$. Instead, since C_1, C_2 are always finite, they can be used conveniently. This is similar to the finite value of the SIF that can be used to evaluate cracks instead of the infinite stress value at the crack tip $\sigma_y(r) \to \infty$ that cannot be used when $r \to 0$. Figure 10 illustrates the values of C_1, C_2 in Fig. 9b when $a/W = 10^{-7}$~10^{-1}, $\alpha = 0.5 \sim 0.95$ under fixed $\beta = 0.3$. Figure 10 shows C_1 and C_2 are insensitive of a/W

Table 4 Values of C_1, C_2 in Eq. (12) having more than three digits accuracy in the range $a/W \leq 10^{-3}$ subjected to tension σ_{y0} in Fig. 9(b) [$K_1 + iK_2 = (F_1 + iF_2)\sigma_{y0}\sqrt{\pi a}(1 + 2i\varepsilon)$, $F_1 = C_1 \cdot (W/a)^{1-\lambda}$, $F_2 = C_2 \cdot (W/a)^{1-\lambda}$]

α	$\beta = -0.2$	$\beta = -0.1$	$\beta = 0$	$\beta = 0.1$	$\beta = 0.2$	$\beta = 0.3$	$\beta = 0.4$	$\beta = 0.45$
Values of C_1								
0	1.071	1.103	1.122	1.103	1.071			
0.05	1.009	1.074	1.114	1.132	1.120			
0.1	0.952	1.034	1.093	1.142	1.166			
0.15	0.881	0.991	1.063	1.138	1.201			
0.2		0.947	1.024	1.119	1.221	1.570		
0.3		0.863	0.938	1.046	1.202	1.530		
0.4		0.786	0.852	0.952	1.113	1.449		
0.5		0.711	0.773	0.857	0.991	1.306		
0.6		0.645	0.702	0.771	0.872	1.103	2.485	
0.7			0.637	0.694	0.769	0.920	1.593	
0.75			0.606	0.659	0.723	0.843	1.297	
0.8			0.576	0.627	0.679	0.777	1.086	1.868
0.85			0.546	0.595	0.640	0.719	0.928	1.408
0.9			0.533	0.565	0.603	0.666	0.815	1.075
0.95			0.519	0.537	0.568	0.619	0.727	0.869
1			0.510	0.500	0.535	0.559	0.644	0.790
Values of C_2								
0	− 0.210	− 0.113	0.000	0.111	0.209			
0.05	− 0.212	− 0.129	− 0.027	0.085	0.198			
0.1	− 0.214	− 0.145	− 0.052	0.059	0.181			
0.15	− 0.209	− 0.157	− 0.074	0.031	0.159			
0.2		− 0.167	− 0.093	0.004	0.133	0.349		
0.3		− 0.178	− 0.123	− 0.046	0.070	0.273		
0.4		− 0.183	− 0.141	− 0.083	0.008	0.181		
0.5		− 0.181	− 0.151	− 0.108	− 0.041	0.089		
0.6		− 0.177	− 0.155	− 0.123	− 0.075	0.013	0.195	
0.7			− 0.155	− 0.132	− 0.095	− 0.037	0.130	
0.75			− 0.153	− 0.134	− 0.102	− 0.054	0.065	
0.8			− 0.151	− 0.135	− 0.107	− 0.067	0.020	0.134
0.85			− 0.147	− 0.136	− 0.111	− 0.076	− 0.012	0.079
0.9			− 0.145	− 0.135	− 0.113	− 0.083	− 0.033	0.024
0.95			− 0.142	− 0.134	− 0.114	− 0.088	− 0.048	− 0.011
1			− 0.139	− 0.129	− 0.101	− 0.087	− 0.061	− 0.026

when $a/W \leq 10^{-1}$ and become almost constant more than three significant digits in the range $a/W \leq 10^{-3}$. It should be noted that when $\alpha = 0.5$, $\alpha = 0.55$ with $\beta = 0.3$, good pair condition $\alpha(\alpha - 2\beta) < 0$ can be satisfied. However, as shown in Fig. 10, the values of C_1, C_2 are also constant for $\alpha = 0.5, 0.55$. In other words, Eq. (12) can also be used for good pairs where singularity disappears. Table 4 shows C_1, C_2 values with more than three digits accuracy in the range $a/W \leq 10^{-3}$ for Fig. 9b under tension σ_{y0} based on the definition (12) . Note that Noda–Lan [8] used another definition, $K_1 = F_1\sigma_{y0}\sqrt{\pi a}$, $K_2 = F_2\sigma_{y0}\sqrt{\pi a}$, $F_1 = C_1 \cdot (W/a)^{1-\lambda}$, $F_2 = C_2 \cdot (W/a)^{1-\lambda}$, and their values are therefore different from the values in Table 4.

Next, consider the SIF of the interface edge crack under uniform stress field in Fig. 9c. The SIFs in Fig. 9c have been also obtained by the proportional method using FEM confirming more than three digits convergence. Figure 11 shows the dimensionless coefficients D_1 and D_2 in Eq. (13) by varying a/W in the range $a/W = 10^{-7}$~10^{-1} and also by varying α in the range $\alpha = 0.5 \sim 0.95$ under fixed $\beta = 0.3$. As shown in Fig. 11, the values of D_1 and D_2 are insensitive of a/W in the range $a/W \leq 10^{-2}$ and coincide with each other more than three significant digits in the range $a/W \leq 10^{-3}$.

$$K_1 + iK_2 = (D_1 + iD_2)\sigma_{y0}\sqrt{\pi a}(1 + 2i\varepsilon) \tag{13}$$

Table 5 shows the values of coefficients D_1, D_2 defined in Eq. (13) having more than three digits accuracy in the range $a/W \leq 10^{-3}$ in Fig. 9c by varying α, β. When $\alpha = 2\beta$, a logarithmic singularity occurs at the interface end and the equivalent load σ_{y0} expressed by Eq. (6) becomes infinite, so Eq. (13) cannot be used although D_1, D_2 are indicated in Table 5. Table 5 shows that the value of D_1 is close to the value of edge crack in homogeneous semi-infinite plate $F_I = 1.1215$.

As shown in Fig. 9, the SIFF_1, F_2 in Fig. 9a can be expressed as Eq. (14) by superposing the problems in Fig. 9b, c. Table 6 indicates C_1, C_2 in Table 4 and D_1, D_2 in Table 5 by taking an example when α

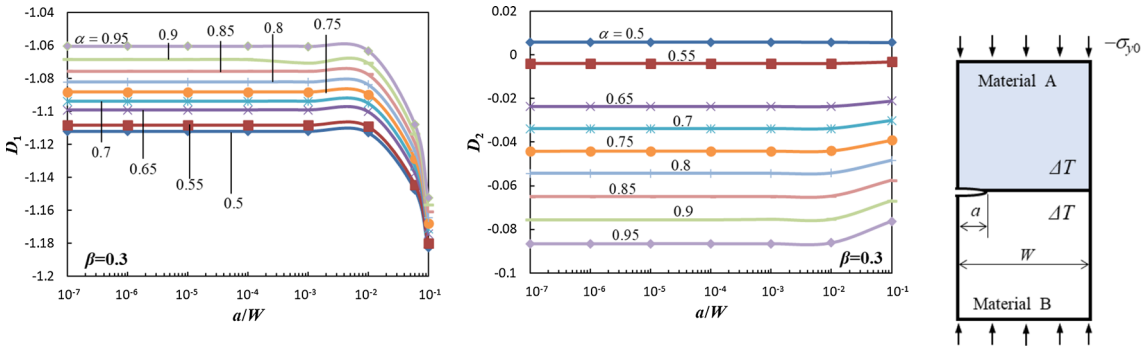

Fig. 11 Values of D_1, D_2 in Fig. 9c by varying a/W in the range $a/W = 10^{-7}$~10^{-1} and also by α in the range $\alpha = 0.5$~0.95 under fixed $\beta = 0.3$ in Fig. 9c

Table 5 Values of D_1, D_2 in Eq. (13) having more than three digits accuracy in the range $a/W \leq 10^{-3}$ subjected to ΔT and σ_{y0} as shown in Fig. 9c [$K_1 + iK_2 = (D_1 + iD_2)\sigma_{y0}\sqrt{\pi a}(1 + 2i\varepsilon)$]

α	$\beta = -0.2$	$\beta = -0.1$	$\beta = 0$	$\beta = 0.1$	$\beta = 0.2$	$\beta = 0.3$	$\beta = 0.4$	$\beta = 0.45$
Values of D_1								
0.00	− 1.127	− 1.123	− 1.122	− 1.123	− 1.127			
0.05	− 1.128	− 1.123	− 1.121	− 1.123	− 1.127			
0.10	− 1.128	− 1.123	− 1.121	− 1.122	− 1.126			
0.15	− 1.128	− 1.123	− 1.120	− 1.121	− 1.124			
0.20		− 1.122	− 1.119	− 1.120	− 1.123	− 1.129		
0.30		− 1.120	− 1.117	− 1.117	− 1.119	− 1.125		
0.40		− 1.117	− 1.113	− 1.112	− 1.114	− 1.119		
0.50		− 1.112	− 1.108	− 1.107	− 1.108	− 1.112		
0.60		− 1.107	− 1.102	− 1.100	− 1.100	− 1.103	− 1.111	
0.70			− 1.094	− 1.091	− 1.091	− 1.094	− 1.100	
0.75			− 1.090	− 1.087	− 1.086	− 1.088	− 1.094	
0.80			− 1.085	− 1.081	− 1.080	− 1.082	− 1.087	− 1.091
0.85			− 1.080	− 1.076	− 1.074	− 1.076	− 1.080	− 1.084
0.90			− 1.074	− 1.070	− 1.068	− 1.069	− 1.072	− 1.076
0.95			− 1.068	− 1.063	− 1.060	− 1.061	− 1.064	− 1.067
1.00			− 1.061	− 1.056	− 1.053	− 1.052	− 1.054	− 1.057
Values of D_2								
0.00	− 0.0647	− 0.0318	0.0000	0.0318	0.0647			
0.05	− 0.0737	− 0.0408	− 0.0089	0.0229	0.0556			
0.10	− 0.0828	− 0.0497	− 0.0179	0.0139	0.0466			
0.15	− 0.0918	− 0.0587	− 0.0268	0.0049	0.0375			
0.20		− 0.0677	− 0.0358	− 0.0041	0.0283	0.0629		
0.30		− 0.0857	− 0.0538	− 0.0222	0.0100	0.0441		
0.40		− 0.1038	− 0.0736	− 0.0405	− 0.0087	0.0251		
0.50		− 0.1221	− 0.0902	− 0.0590	− 0.0274	0.0058		
0.60		− 0.1407	− 0.1089	− 0.0778	− 0.0465	− 0.0140	0.0217	
0.70			− 0.1278	− 0.0970	− 0.0660	− 0.0338	0.0009	
0.75			− 0.1374	− 0.1067	− 0.0759	− 0.0440	− 0.0097	
0.80			− 0.1472	− 0.1166	− 0.0860	− 0.0544	− 0.0206	− 0.0020
0.85			− 0.1571	− 0.1266	− 0.0962	− 0.0649	− 0.0314	− 0.0132
0.90			− 0.1671	− 0.1368	− 0.1066	− 0.0756	− 0.0425	− 0.0248
0.95			− 0.1774	− 0.1472	− 0.1172	− 0.0865	− 0.0539	− 0.0363

$= 0.8$, 0.9, $\beta = 0.3$. By substituting those values into Eq. (14), the values of $F_1 = C_1 \cdot (W/a)^{1-\lambda} + D_1$, $F_2 = C_2 \cdot (W/a)^{1-\lambda} + D_2$ are estimated and indicated in Table 6 as "F_1 in Eq. (14)" and "F_2 in Eq. (14)."

$$K_1 + iK_2 = (F_1 + iF_2)\sigma_{y0}\sqrt{\pi a}(1 + 2i\varepsilon),\ F_1 = C_1 \cdot (W/a)^{1-\lambda} + D_1,$$
$$F_2 = C_2 \cdot (W/a)^{1-\lambda} + D_2, \tag{14}$$

when $\alpha(\alpha - 2\beta) > 0$, $\quad a/W \leq 10^{-3}$in Fig. 9a

To confirm the validity those values, the proportional method described in Sect. 3.1 is applied and the obtained F_1, F_2 values are indicated in Table 6 as "Proportional method." It is seen that F_1, F_2 values from

Table 6 Confirmation of F_1, F_2 values estimated from Table 4 and Table 5 coincident with the results obtained by the proportional method $[K_1 + iK_2 = (F_1 + iF_2)\sigma_{y0}\sqrt{\pi a}(1 + 2i\varepsilon)]$

$\beta = 0.3$	F_1					F_2			
α	a/W	C_1 in Table 4	D_1 in Table 5	F_1 from Eq.(14)	Proportional method	C_2 in Table 4	D_2 in Table 5	F_2 from Eq. (14)	Proportional method
0.8	10^{-6}	0.777	− 1.0822	3.892	3.8918	− 0.067	− 0.0544	− 0.476	− 0.4757
	10^{-5}	0.777	− 1.0822	2.568	2.5675	− 0.067	− 0.0544	− 0.364	− 0.3635
	10^{-4}	0.777	− 1.0822	1.596	1.5956	− 0.067	− 0.0544	− 0.281	− 0.2813
0.9	10^{-6}	0.666	− 1.0683	10.38	10.380	− 0.083	− 0.0756	− 1.491	− 1.491
	10^{-5}	0.666	− 1.0683	6.058	6.0577	− 0.083	− 0.0756	− 0.957	− 0.9567
	10^{-4}	0.666	− 1.0683	3.367	3.3671	− 0.083	− 0.0756	− 0.624	− 0.6242

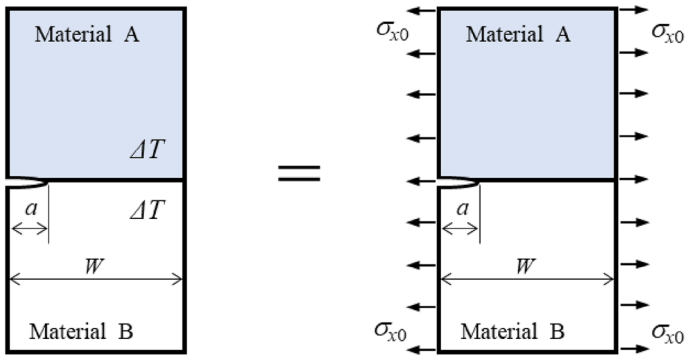

(a) (b)

Fig. 12 Singular interface stress due to thermal loading expressed by the equivalent tensile stress in the$x$-direction $\sigma_{x0}$when $\alpha - 2\beta = 0$ **a** the thermal loading in bimaterial plate **b** tensile loading in the$x$-direction

C_1, C_2, D_1, D_2 and F_1, F_2 values from proportional method coincide with each other more than three significant digits. In this way, it is confirmed that Table 4 and Table 5 are useful for obtained the SIF in Fig. 9a.

4.2 Stress intensity factor of an edge crack in a wide bimaterial plate considering the logarithmic singular stress field without crack

Regarding the singularity at the joint end, it is known that a logarithmic singular stress field occurs as shown in Fig. 12 when $\alpha - 2\beta = 0$ in terms of Dundurs parameter [10, 13]. Furthermore, when $\alpha - 2\beta = 0$, the equivalent tensile stress σ_{y0} defined in Eq. (6) goes to infinity although σ_{y0} can be used to express the thermal singular stress field as shown in Fig. 9a when $\alpha - 2\beta \neq 0$. Therefore, instead of σ_{y0}, the uniform temperature change is expressed by applying the stress σ_{x0} defined in Eq. (15) in the$x$-direction as shown in Fig. 12. As shown in Appendix C, the equivalent stress σ_{x0} of Eq. (15) can be derived from the condition that the strain ε_x at the interface is equal between the upper and lower materials [6, 18].

$$\sigma_{x0} = \frac{8G_A G_B\left(\eta_B^* - \eta_A^*\right)\Delta T}{G_A(\kappa_B + 1) - G_B(\kappa_A + 1)} \tag{15}$$

The equivalent stress replacement in Fig. 12 by using σ_{x0} defined in Eq. (15) is useful not only when $\alpha - 2\beta = 0$, but also for all material combinations α, β [11]. However, the replacement in Fig. 12 cannot clarify the difference between the tensile load and the thermal load unlike the replacement in Fig. 9 by using σ_{y0} defined in Eq. (15). Therefore, it is inconvenient to use the replacement in Fig. 12b as well as the direct analysis results of the thermal load in Fig. 12a itself especially in experiments that combine thermal loads and tensile loads conducted previously. In other words, the substitution method in Fig. 9 is more useful than the one in Fig. 12 for the previous experiments combining thermal and tensile loads [5, 6]. Therefore, this paper uses the replacement in Fig. 12 only when $\alpha - 2\beta = 0$.

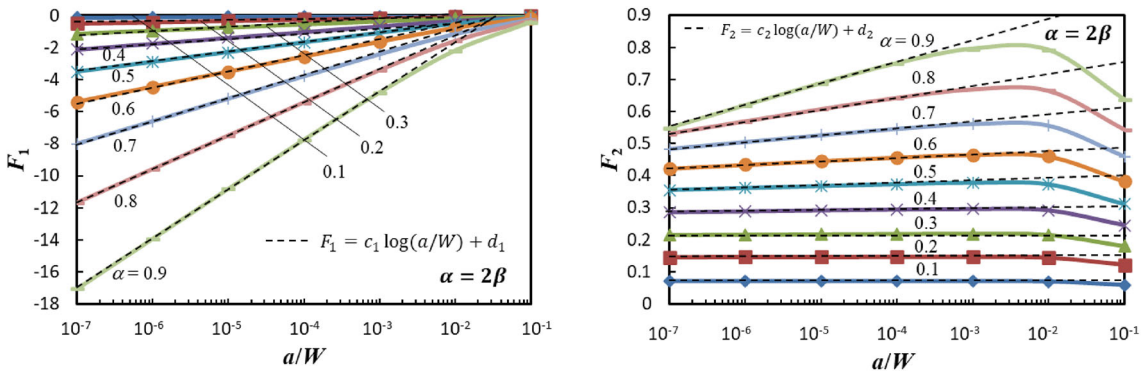

Fig. 13 Relation between F_1, F_2 and the relative crack length a/W in Fig. 12 when $\alpha - 2\beta = 0$

Figure 13 shows the stress intensity factors F_1, F_2 vs. log (a/W) relation. Figure 13 indicates F_1, F_2 of edge cracks are controlled by interface edge logarithmic singularity when there is no crack. Then, they are proportional to log (a/W) when $a/W \leq 10^{-3}$. Therefore, as shown in the dashed line in Fig. 13 when $a/W \leq 10^{-3}$, F_1, F_2 can be expressed by Eq. (16).

$$K_1 + iK_2 = (F_1 + iF_2)\sigma_{x0}\sqrt{\pi a}(1 + 2i\varepsilon),\ F_1 = c_1 \log(a/W) + d_1,$$
$$F_2 = c_2 \log(a/W) + d_2, \tag{16}$$

where $(\alpha - 2\beta) = 0$, $a/W \leq 10^{-3}$ in Fig. 12a

As shown in Fig. 14, the values of c_1, c_2, d_1, d_2 are insensitive of a/W in the range $a/W \leq 10^{-2}$ and coincide with each other more than three significant digits in the range $a/W \leq 10^{-3}$. Figure 15 shows the values of c_1, c_2, d_1, d_2 obtained by the proportional method in the whole range of α. Since those values depend on only α (= 2β), they can be approximated as a function of α as shown in Eq. (17), which can be conveniently used to obtain the values c_1, c_2, d_1, d_2 for any value of α. They are odd functions with respect to α. It is confirmed that the calculation formula (17) may provide F_1, F_2 values with less than 1% error.

$$\begin{aligned} c_1 &= 10.7035\alpha^6 - 20.9471\alpha^5 + 18.3439\alpha^4 - 6.6708\alpha^3 + 3.2555\alpha^2 - 0.0671\alpha \\ c_2 &= 0.3721\alpha^6 - 0.6765\alpha^5 + 0.5463\alpha^4 - 0.1638\alpha^3 + 0.0334\alpha^2 - 0.0022\alpha \\ d_1 &= -25.5432\alpha^6 - 49.8314\alpha^5 - 41.8688\alpha^4 - 15.1837\alpha^3 - 4.9974\alpha^2 - 0.1509\alpha \\ d_2 &= 4.0137\alpha^6 - 9.6898\alpha^5 + 9.4712\alpha^4 - 4.0005\alpha^3 + 0.8521\alpha^2 + 0.6590\alpha \end{aligned} \tag{17a}$$

where $\alpha = 2\beta \geq 0$, $a/W \leq 10^{-3}$

$$\begin{aligned} c_1 &= -10.7035\alpha^6 - 20.9471\alpha^5 - 18.3439\alpha^4 - 6.6708\alpha^3 - 3.2555\alpha^2 - 0.0671\alpha \\ c_2 &= -0.3721\alpha^6 - 0.6765\alpha^5 - 0.5463\alpha^4 - 0.1638\alpha^3 - 0.0334\alpha^2 - 0.0022\alpha \\ d_1 &= -25.5432\alpha^6 - 49.8314\alpha^5 - 41.8688\alpha^4 - 15.1837\alpha^3 - 4.9974\alpha^2 - 0.1509\alpha \\ d_2 &= -4.0137\alpha^6 - 9.6898\alpha^5 - 9.4712\alpha^4 - 4.0005\alpha^3 - 0.8521\alpha^2 + 0.6590\alpha \end{aligned} \tag{17b}$$

where $\alpha = 2\beta \leq 0$, $a/W \leq 10^{-3}$.

Finally, Table 7 summarizes suitable expressions considering the double singular stress fields in Fig. 9 under mechanical loading and thermal loading. Even when F_1, $F_2 \to \infty$, the coefficients C_1,C_2,D_1,D_2,c_1,c_2,d_1, d_2 are always finite and suitable to express F_1, F_2. This is similar to the finite value of the stress intensity factors that can be used to evaluate cracks instead of the infinite stress value at the crack tip $\sigma_y(r) \to \infty$ that cannot be used when $r \to 0$. In Table 7, the expressions of F_1, F_2 are chosen to express the singular stress fields considering the difference between thermal loading and mechanical loading.

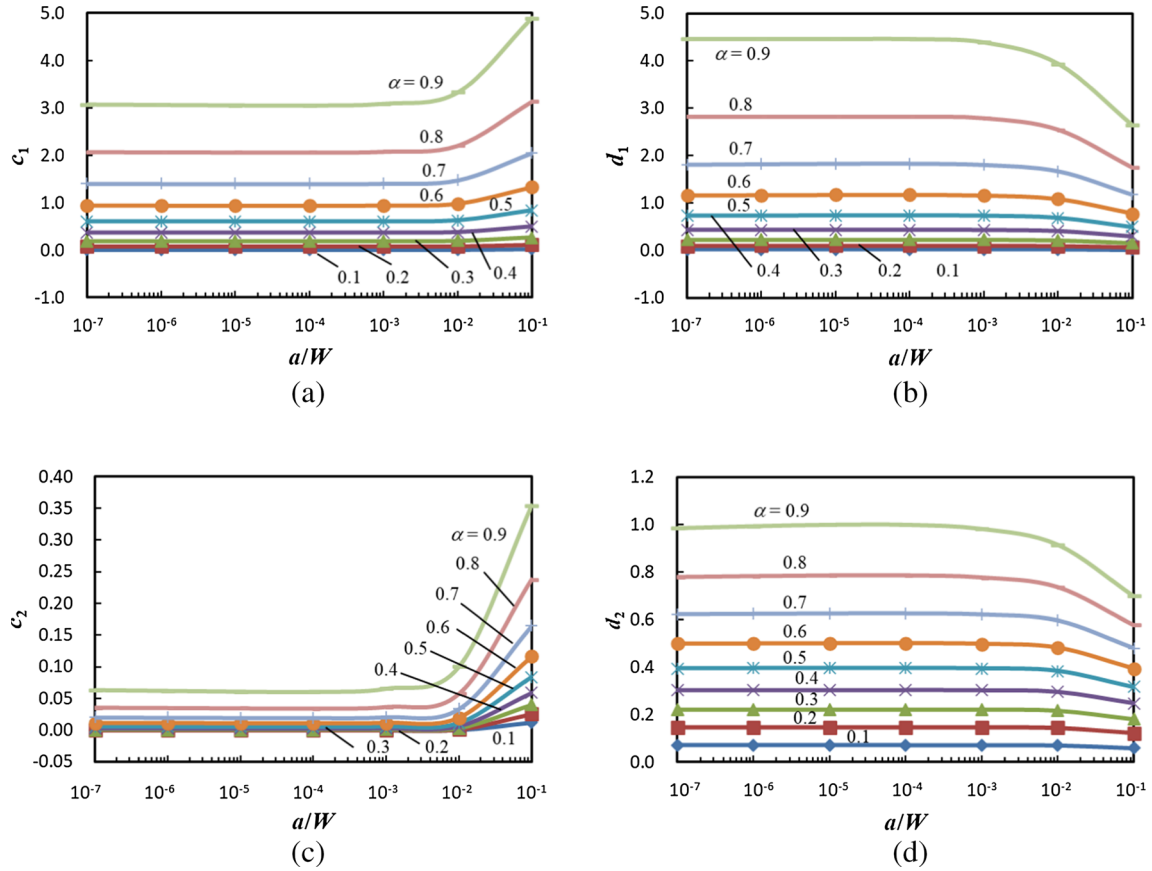

Fig. 14 Relation between c_1, d_1, c_2, d_2 and the relative crack length a/W in Fig. 12 when $\alpha - 2\beta = 0$

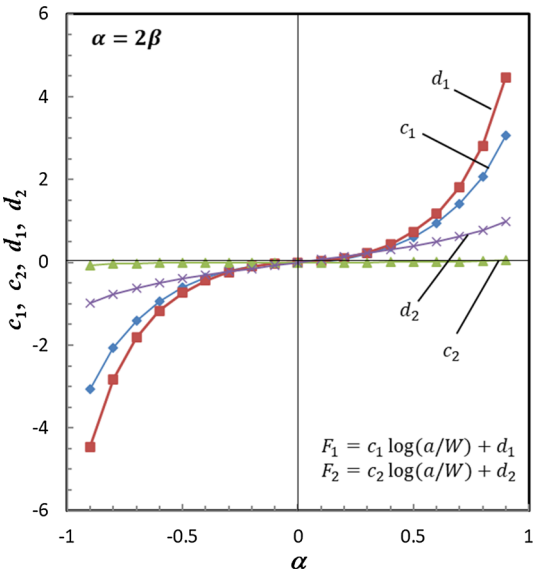

Fig. 15 Valuses of c_1, c_2, d_1, d_2 in Eq. (17) when $-0.9 \leq \alpha(= 2\beta) \leq 0.9$

Table 7 Suitable expression of F_1, F_2 in Fig. 9 when $a/W \leq 10^{-3}$ considering the double singular stress fields in Fig. 9 under mechanical loading and thermal loading. [$K_1 + iK_2 = (F_1 + iF_2)\sigma_0\sqrt{\pi a}(1 + 2i\varepsilon)$, σ_0 is the equivalent stress defined by Eq. (6) or Eq. (15)]

Material combination	Under thermal loading		Under mechanical loading	
	Edge singularity	Dimensionless SIFs	Edge singularity	Dimensionless SIFs
$\alpha(\alpha - 2\beta) > 0$ (bad pair)	$0 < \lambda < 1$	$F_1 = C_1 \cdot (W/a)^{1-\lambda} + D_1 \to \infty\ (a/W \to 0)$ $F_2 = C_2 \cdot (W/a)^{1-\lambda} + D_2 \to \infty\ (a/W \to 0)$	$0 < \lambda < 1$	$F_1 = C_1 \cdot (W/a)^{1-\lambda} \to \infty\ (a/W \to 0)$ $F_2 = C_2 \cdot (W/a)^{1-\lambda} \to \infty\ (a/W \to 0)$
$\alpha(\alpha - 2\beta) = 0$ (equal pair)	$\log(r)$ $(\alpha \neq 0)$	$F_1 = c_1 \log(a/W) + d_1 \to \infty\ (a/W \to 0)$ $F_2 = c_2 \log(a/W) + d_2 \to \infty\ (a/W \to 0)$	$\lambda = 1$	$F_1 = \text{finite} = C_1\ (a/W \to 0)$ $F_2 = \text{finite} = C_2\ (a/W \to 0)$
$\alpha(\alpha - 2\beta) < 0$ (good pair)	$\lambda > 1$	$F_1 = C_1 \cdot (W/a)^{1-\lambda} + D_1 \to D_1\ (a/W \to 0)$ $F_2 = C_2 \cdot (W/a)^{1-\lambda} + D_2 \to D_2\ (a/W \to 0)$	$\lambda > 1$	$F_1 = C_1 \cdot (W/a)^{1-\lambda} \to 0\ (a/W \to 0)$ $F_2 = C_2 \cdot (W/a)^{1-\lambda} \to 0\ (a/W \to 0)$

5 Conclusions

In recent years, mechanical failures due to thermal stress such as cracking and delamination at the interface of dissimilar materials are becoming more problematic in automobiles, computers, etc. To evaluate such thermal load-induced damage in terms of the singular stress field, it is necessary to consider a constant term as well as the singular term at the interface end, unlike in the case of mechanical loading. In this study, therefore, the stress intensity factors (SIFs) of an interface edge crack in a wide bimaterial plate due to uniform temperature change were analyzed and they were indicated under arbitrary material combination. It was confirmed that the values are independent of the crack length when the crack length is sufficiently small when the relative crack length $a/W \leq 10^{-3}$. The conclusion can be summarized as follows.

Care should be taken for the SIF under thermal loading when $\alpha(\alpha - 2\beta) = 0$ and $\alpha(\alpha - 2\beta) < 0$ (see Table 7). When $\alpha(\alpha - 2\beta) = 0$, the dimensionless SIF F_1, $F_2 \to \infty$ as $a/W \to 0$ under thermal loading although F_1, $F_2 \to$ finite under mechanical loading. When $\alpha(\alpha - 2\beta) < 0$, F_1, $F_2 \to$ finite as $a/W \to 0$ under thermal loading although F_1, $F_2 \to 0$ under mechanical loading.

When $\alpha - 2\beta \neq 0$ and $a/W \leq 10^{-3}$ in Fig. 9a, the SIF under uniform temperature change can be expressed by superposing the SIF under tension in Fig. 9b and the SIF due to a uniform interface stress in Fig. 9c as shown in the following equations.

$$K_1 + iK_2 = (F_1 + iF_2)\sigma_{y0}\sqrt{\pi a}(1 + 2i\varepsilon),\ F_1 = C_1(W/a)^{1-\lambda} + D_1,\ F_2 = C_2(W/a)^{1-\lambda} + D_2$$

$$\sigma_{y0} = \frac{8G_AG_B\left(\eta_B^* - \eta_A^*\right)\Delta T}{G_A(\kappa_B - 1) - G_B(\kappa_A - 1) - 2(G_A - G_B)},$$

$$\eta_m^* = \begin{cases} \eta_m & \text{(plane stress)} \\ (1 + \nu_m)\,\eta_m & \text{(plane strain)} \end{cases} (m = A,\ B)$$

In this study, the coefficients C_1,C_2, D_1, D_2 are tabulated in Tables 4, 5 in the whole range of α, β. The values of C_1,C_2, D_1, D_2 are insensitive of a/W in the range $a/W \leq 10^{-2}$ and coincide with each other more than three significant digits in the range $a/W \leq 10^{-3}$. Therefore, the SIFs of the thermal stress field were presented under arbitrary material combinations.

When $\alpha - 2\beta = 0$ and $a/W \leq 10^{-3}$ in Fig. 12a, due to the peculiar logarithmic singularity under thermal loading, the SIF of an interfacial edge crack in a bonded plate under uniform temperature change in Fig. 12a can be expressed in the following equations.

$$K_1 + iK_2 = (F_1 + iF_2)\sigma_{x0}\sqrt{\pi a}(1 + 2i\varepsilon),\ F_1 = c_1\log(a/W) + d_1,\ F_2 = c_2\log(a/W) + d_2$$

$$\sigma_{y0} = \frac{8G_AG_B\left(\eta_B^* - \eta_A^*\right)\Delta T}{G_A(\kappa_B + 1) - G_B(\kappa_A + 1)},$$

$$\eta_m^* = \begin{cases} \eta_m & \text{(plane stress)} \\ (1+\nu_m)\,\eta_m & \text{(plane strain)} \end{cases} (m = A,\ B)$$

The values of c_1, c_2, d_1, d_2 are insensitive of a/W in the range $a/W \leq 10^{-2}$ and coincide with each other more than three significant digits in the range $a/W \leq 10^{-3}$. In this study, the coefficients c_1, c_2, d_1, d_2 are expressed in Eq. (17), which can be used conveniently in the whole range of α $(= 2\beta)$ with less than 1% error.

Suitable expressions of F_1, F_2 are summarized in Table 7 by considering the double singular stress fields in Fig. 9 under arbitrary material combination. It should be noted that even when F_1, $F_2 \to \infty$, the coefficients $C_1, C_2, D_1, D_2, c_1, c_2, d_1, d_2$ are always finite and suitable to express F_1, F_2. This is similar to the finite value of the stress intensity factors that can be used to evaluate cracks instead of the infinite stress value at the crack tip $\sigma_y(r) \to \infty$ that cannot be used when $r \to 0$. In Table 7, the expressions of F_1, F_2 are chosen to express the singular stress fields considering the difference between thermal loading and mechanical loading.

Acknowledgements The authors wish to thank Mr Kyohei Takeda for his assistance in the numerical calculations of some problems. This work was partially supported by Japan Society for the Promotion of Science, JSPS KAKENHI Grant Number JP 21K03818.

Appendix A. Mesh independence of interface stress intensity factor obtained by the proportional method

The proportional method is useful for analyzing interface cracks by providing mesh-independent interface SIFs efficiently. Since the FEM results are mesh-independent, the obtained results can be regarded as the exact solution by using the exact reference solution. The detail of the accuracy discussion can be found in previous papers under mechanical loading [8, 15, 16]. For the readers' convenience, in this paper, several examples of mesh independence will be shown by varying the minimum element size e/a under thermal and mechanical loading.

Table 8 shows the SIFs F_1, F_2 of the short and long edge cracks in the bimaterial plate when $a/W = 10^{-5}$ and $a/W = 0.8$. By varying the minimum element size e/a around the crack, the SIFs are indicated under thermal and mechanical loading. The four-node quadrilateral elements are used and the minimum element sizes are $e/a = 3^{-6}/11,\ 3^{-7}/11,\ 3^{-8}/11$ for each FE model. The FEM mesh around the crack tip in the reference problem is the same as that of the unknown problem. In the analysis, the elastic parameters are fixed as $\alpha = 0.8$ and $\beta = 0.3$. Table 8 shows that the results of F_1, F_2 are mesh-independent to more than three digits for both short and long cracks. Under the thermal loading, the proportional method provides the same level of accuracy under the mechanical loading. The expression $F_1 = C_1(W/a)^{1-\lambda} + D_1$, $F_2 = C_2(W/a)^{1-\lambda} + D_2$ is significant in thermal loading since the SIF of a larger crack is always smaller (see Appendix B).

The coefficients C_1, C_2, D_1, D_2 in Eq. 14 can be analyzed by applying the proportional method on the basis of the illustration in Fig. 9a–c. Table 9 shows that the results of F_1, F_2 are mesh-independent to more than three digits when $a/W = 10^{-5}$ and 10^{-7}. All values of C_1, C_2, D_1, D_2 in Table 4 and Table 5 are obtained by confirming more than three digits accuracy as shown in Table 9. As shown in Table 9, C_1, C_2, D_1, D_2 are useful for expressing short cracks because the constant values can be used for $a/W \leq 10^{-3}$. Instead, F_1, F_2 increase with decreasing a/W.

See Tables 8 and 9.

Table 8 Mesh− independence of F_1, F_2 obtained by the proportional method in Fig. 9a, b ($K_1 + iK_2 = (F_1 + iF_2)\sigma_{y0}\sqrt{\pi a}(1+2i\varepsilon)$, $\alpha = 0.8$, $\beta = 0.3$, $a/W = 10^{-5}$ and $a/W = 0.8$)

a/W	e/a	Thermal loading		Mechanical loading	
		F_1	F_2	F_1	F_2
10^{-5}	$3^{-6}/11$=1/8019	2.5714	− 0.3636	3.6521	− 0.3095
	$3^{-7}/11$=1/24057	2.5704	− 0.3635	3.6522	− 0.3096
	$3^{-8}/11$=1/72171	2.5705	− 0.3635	3.6539	− 0.3097
0.8	$3^{-6}/11$=1/8019	− 0.00265	− 0.03099	11.856	− 1.3787
	$3^{-7}/11$=1/24057	− 0.00264	− 0.03099	11.860	− 1.3780
	$3^{-8}/11$=1/72171	− 0.00263	− 0.03102	11.861	− 1.3765

Table 9 Mesh− independence of C_1, C_2, D_1, D_2 obtained by the proportional method in Fig. 9b , c ($K_1 + iK_2 = (F_1 + iF_2)\sigma_{y0}\sqrt{\pi a}(1 + 2i\varepsilon)$, $\alpha = 0.8$, $\beta = 0.3$)

a/W	e/a	Figure 9a		Figure 9b		Figure 9c	
		F_1*	F_2*	C_1	C_2	D_1	D_2
10^{-5}	1/8019	2.5711	− 0.3636	0.7773	− 0.0658	− 1.0839	− 0.05423
	1/24057	2.5706	− 0.3643	0.7768	− 0.0659	− 1.0821	− 0.05438
	1/72171	2.5701	− 0.3642	0.7767	− 0.0658	− 1.0821	− 0.05437
10^{-7}	1/8019	5.7031	− 0.6286	0.7768	− 0.0658	− 1.0816	− 0.05436
	1/24057	5.7001	− 0.6284	0.7765	− 0.0657	− 1.0820	− 0.05437
	1/72171	5.6991	− 0.6283	0.7764	− 0.0657	− 1.0821	− 0.05439

*In Table 9, F_1^*, F_2^* are obtained from $F_1^* = C_1 \cdot (W/a)^{1-\lambda} + D_1$, $F_2^* = C_2 \cdot (W/a)^{1-\lambda} + D_2$

Appendix B. Stress intensity factor solution of an edge interface crack in a bimaterial plate under thermal and mechanical loading in the whole range $a/W = 0 \sim 1.0$

The stress intensity factor (SIF) was previously analyzed for an edge interface crack in a bimaterial plate subjected to tension σ_0 in Fig. 1 by varying material combinations systematically [7, 8]. Figure 16a shows some examples of F_1-a/W relations as well as K_1-a/W relations when$\alpha = 0.4 \sim 0.95$ under fixed $\beta = 0.3$. As shown Fig.16a, $F_1 \to \infty$ as $a/W \to 0$ when $\alpha(\alpha - 2\beta) > 0$. Figure 16b shows the log–log plot of F_1-a/W relations to confirm the double singular stress behavior of F_1 in detail. According to Fig. 16b, it can be seen that F_1 can be expressed as shown in Eq. (B1) in the range of $a/W \leq 10^{-3}$. Here, λ is the singularity index at the interface end without crack.

$$F_1 = C_1 \cdot (W/a)^{1-\lambda} \tag{B1}$$

In other words, Fig. 16b shows that the dimensionless stress intensity factor $F_1 = C_1(W/a)^{1-\lambda}$ is controlled by the singular stress field without crack, which can be expressed as shown in Eq. (1), that is, $\sigma_y(r) = K_\sigma / r^{1-\lambda}$. As shown in Fig. 10, the values of C_1 and C_2 are independent of a/W and coincide with each other more than four significant digits in the range $a/W \leq 10^{-3}$. In the previous studies, the SIF solution when $a/W \leq 10^{-3}$ in Fig.16 was provided under arbitrary material combinations. The SIFs are expressed by considering the character of the double singular stress field as shown in Eq. (B2).

$K_1 + iK_2 = (F_1 + iF_2)\sigma_0\sqrt{\pi a}(1 + 2i\varepsilon)$ in Fig. 1 when $a/W \leq 10^{-3}$:

$$\begin{cases} \text{When } \alpha(\alpha - 2\beta) > 0: \ F_1 = C_1(W/a)^{1-\lambda}, F_2 = C_2(W/a)^{1-\lambda}, C_1, C_2 \to \text{finite } (a/W \to 0), 0 < \lambda < 1 \\ \text{When } \alpha(\alpha - 2\beta) = 0: \ F_1 = C_1 = 1.121 + 0.0128\beta - 0.253\beta^2, F_2 = C_2 = 0.029\beta + 0.0526\beta^2, \lambda = 1 \\ \text{When } \alpha(\alpha - 2\beta) < 0: \ F_1 = C_1(W/a)^{1-\lambda}, F_2 = C_2(W/a)^{1-\lambda}, C_1, C_2 \to \text{finite } (a/W \to 0), \lambda > 1 \end{cases} \tag{B2}$$

Figure 16c shows some examples of $K_1 - a/W$ relations subjected to the remote tensile stress $\sigma_0 = 1$ when $\alpha = 0.4 \sim 0.95$ under fixed $\beta = 0.3$. As shown Fig.16c, the stress intensity factor K_1 increases with increasing the relative crack length a/W. The value of K_2 also increases with increasing a/W in a similar way of K_1.

See Fig. 16.

Table 10 shows the SIFs F_1, F_2 of the edge crack in the bimaterial plate subjected to thermal and mechanical loading analyzed for various crack sizes $a/W = 10^{-5} \sim 0.8$. For thermal loading, F_1, F_2 decrease rapidly with increasing a/W. Therefore, the expression $F_1 = C_1(W/a)^{1-\lambda} + D_1$, $F_2 = C_2(W/a)^{1-\lambda} + D_2$ is significant in thermal loading since the SIF of a larger crack is always smaller.

See Table 10.

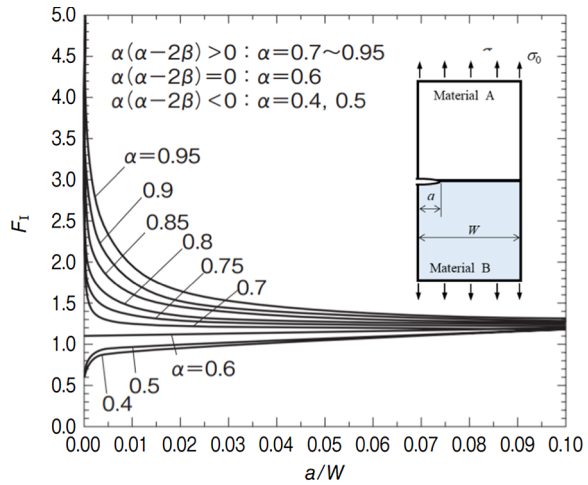

(a)

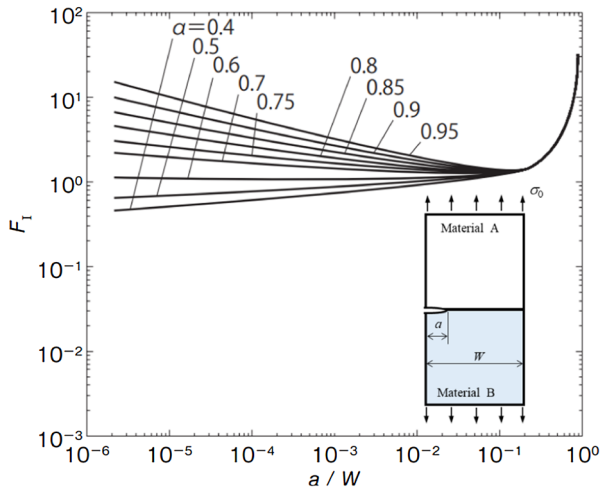

(b)

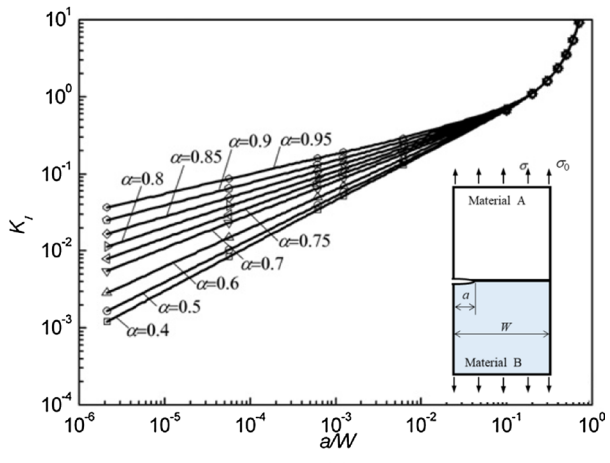

(c)

Fig. 16 F_1 in Eq. B1 as $K_1 + iK_2 = (F_1 + iF_2)\sigma_0\sqrt{\pi a}(1 + 2i\varepsilon)$ for an edge interface crack in a bimaterial plate when $\alpha = 0.4 \sim 0.95$ under fixed $\beta = 0.3$

Table 10 SIFs F_1, F_2 in 9a, b in the range $a/W = 10^{-5} \sim 0.8$ ($K_1 + iK_2 = (F_1 + iF_2)\sigma_{y0}\sqrt{\pi a}(1 + 2i\varepsilon)$, $\alpha = 0.8$, $\beta = 0.3$)

a/W	Thermal loading		Mechanical loading	
	F_1	F_2	F_1	F_2
10^{-5}	2.5675	− 0.3635	3.6496	− 0.3091
10^{-4}	1.5956	− 0.2813	2.6777	− 0.2269
10^{-3}	0.8830	− 0.2214	1.9651	− 0.1671
10^{-2}	0.37239	− 0.1776	1.4562	− 0.12330
0.1	0.06995	− 0.13148	1.2440	− 0.0831
0.2	0.02854	− 0.10759	1.3798	− 0.0724
0.3	0.01443	− 0.08947	1.6624	− 0.0747
0.4	0.00731	− 0.07438	2.1080	− 0.0930
0.5	0.00338	− 0.06183	2.8154	− 0.1389
0.6	0.00062	− 0.05086	3.9980	− 0.2446
0.8	− 0.00264	− 0.03099	11.856	− 1.3787

Appendix C. Derivation of equivalent stress σ_{y0} and σ_{x0} to express thermal singular stress field

In this study, the equivalent stress is used to express the stress intensity factor of the edge interfacial crack under the thermal loading [6]. Then, the equivalent tensile stress σ_{y0} acting in the$y$-direction defined in Eq. (6) is used to express the power-type singularity $r^{\lambda-1}$ at the interface end, and the equivalent tensile stress σ_{x0} acting in the$x$-direction defined in Eq. (15) is used to express the logarithmic-type singularity at the interface end.

See Fig. 17.

Figure 17 illustrates that the stress field due to a uniform temperature change ΔT in Fig. 17a can be expressed by superposing the stress fields caused by the boundary conditions in Fig. 17d,e. Figure 17a shows a bonded strip subjected to a uniform temperature change of ΔT. As shown in Fig. 17b, if both materials are separated from each other, a difference of thermal strain along the interface, $\varepsilon^T_{x,A} - \varepsilon^T_{x,B}$, is produced because of the difference of the thermal expansion coefficients. This difference can be canceled by applying a certain uniform pressure $\sigma_y = -\sigma_{y0}$ to those plates, as shown in Fig. 17c. Assuming that the difference due to the uniform pressure $\sigma_y = -\sigma_{y0}$ is equal to $\varepsilon^\sigma_{x,A} - \varepsilon^\sigma_{x,B}$, the condition along the interface in Fig. 17c can be expressed in Eq. (C1).

$$\varepsilon^T_{x,A} - \varepsilon^T_{x,B} - \left(\varepsilon^\sigma_{x,A} - \varepsilon^\sigma_{x,B}\right) = 0 \rightarrow \left(\eta^*_A - \eta^*_B\right)\Delta T - \left(-\frac{\nu^*_A}{E^*_A} + \frac{\nu^*_B}{E^*_B}\right)\sigma_{y0} = 0 \tag{C1}$$

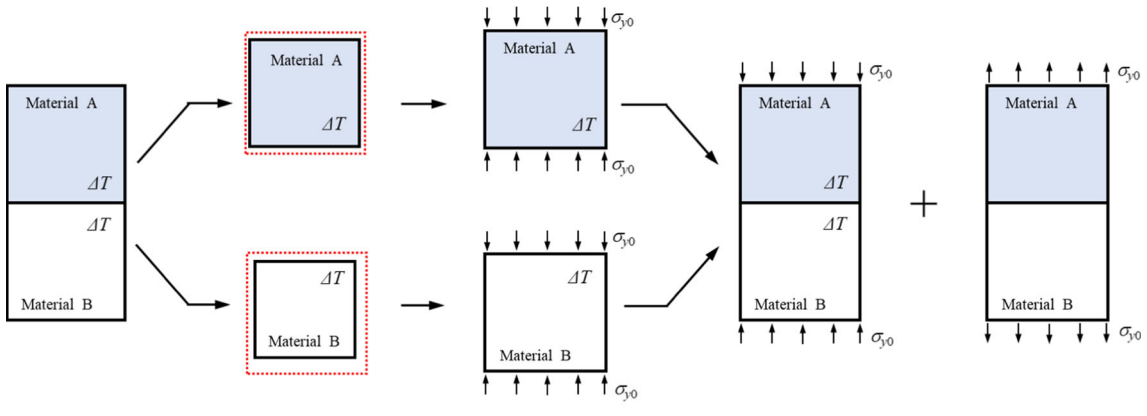

Fig. 17 Singular stress field caused by temperature change is equivalent to that caused by uniaxial tension in the$y$-direction

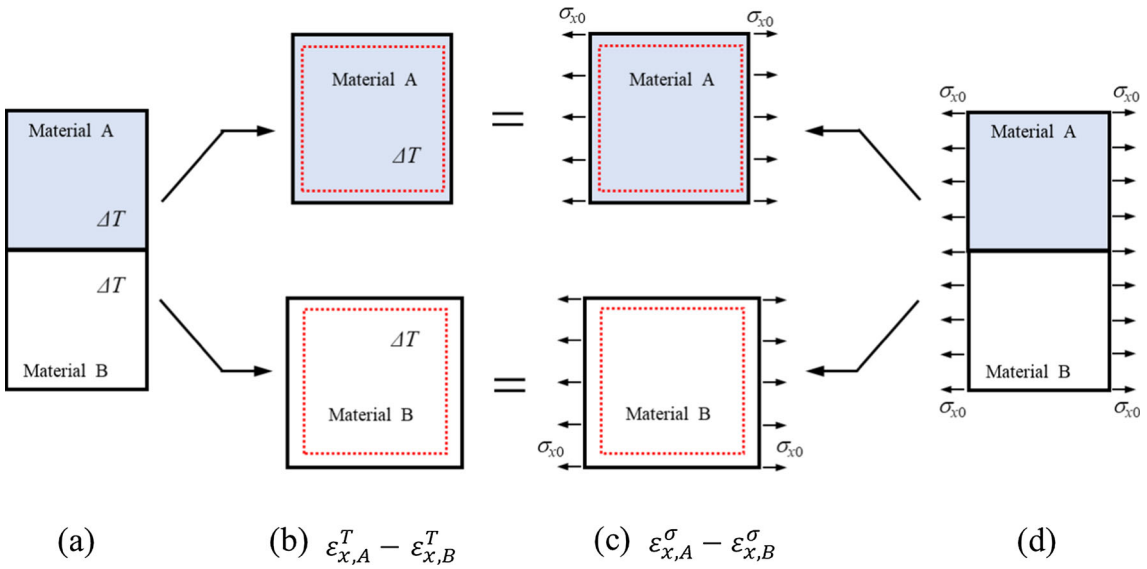

Fig. 18 Singular stress field caused by temperature change is equivalent to that caused by uniaxial tension in the$x$-direction

As shown in Fig. 17d, two plates have no difference in the width of interface and can be bonded to each other. In order to be the same as the boundary conditions in Fig. 17a, an additional tensile stress $\sigma_y = \sigma_{y0}$ should be applied in Fig. 17e. Therefore, the equivalent stress σ_{y0} can be expressed in Eq. (C2).

$$\sigma_{y0} = \frac{(\eta^*_B - \eta^*_A)\Delta T}{\frac{\nu^*_B}{E^*_B} - \frac{\nu^*_A}{E^*_A}} \tag{C2}$$

Equation (C2) can be written as shown in Eq. (C3) by using the relations $E_m = 2(1 + \nu_m)G_m$ and $\kappa_m = (3 - \nu_m)/(1 + \nu_m)$ for plane stress, $\kappa_m = 3 - 4\nu_m$ for plane strain (m = A, B).

$$\sigma_{y0} = \frac{8G_A G_B\left(\eta^*_B - \eta^*_A\right)\Delta T}{G_A(\kappa_B - 1) - G_B(\kappa_A - 1) - 2(G_A - G_B)},$$
$$\eta^*_m = \begin{cases} \eta_m & \text{(plane stress)} \\ (1 + \nu_m)\eta_m & \text{(plane strain)} \end{cases} (m = A, B) \tag{C3}$$

When $\alpha - 2\beta = 0$, the logarithmic singularity occurs near the interface end. As shown in Eq. (C4), the denominator of Eq. (C3) becomes zero, and the equivalent stress σ_{y0} cannot be applied.

$$\alpha - 2\beta = 0 \rightarrow G_A(\kappa_B - 1) - G_B(\kappa_A - 1) - 2(G_A - G_B) = 0 \tag{C4}$$

See Fig. 18.

Figure 18 illustrates that the stress field due to a uniform temperature change ΔT in Fig. 18a can be expressed as the one due to the equivalent tensile stress in the$x$-direction. As shown in Fig. 18b, if both materials are separated from each other, a difference of thermal strain along the interface, $\varepsilon^T_{x,A} - \varepsilon^T_{x,B}$, is produced because of the difference of the thermal expansion coefficients. Fig. 18c shows that the same difference can also be produced by applying a certain uniform tension in the$x$-direction to those plates as shown in Eq. (C5).

$$\varepsilon^T_{x,A} - \varepsilon^T_{x,B} = \varepsilon^\sigma_{x,A} - \varepsilon^\sigma_{x,B} \rightarrow (\eta^*_A - \eta^*_B)\Delta T = \left(\frac{1}{E^*_A} - \frac{1}{E^*_B}\right)\sigma_{x0} \tag{C5}$$

Therefore, the equivalent stress σ_{x0} in the$x$-direction can be expressed in Eq. (C6).

$$\sigma_{x0} = \frac{(\eta^*_B - \eta^*_A)\Delta T}{\frac{1}{E^*_B} - \frac{1}{E^*_A}} = \frac{8G_A G_B\left(\eta^*_B - \eta^*_A\right)\Delta T}{G_A(\kappa_B + 1) - G_B(\kappa_A + 1)} \tag{C6}$$

References

1. Hattori, T., Sakata, S., Hatsuda, T., Murakami, G.: A stress singularity parameters approach for evaluating adhesive strength. JSME Int. J. Ser. I **31**(4), 718–723 (1988)
2. Kuo, A.Y.: Thermal stresses at the edge of a bimetallic thermostat. J. Appl. Mech. **56**, 585–589 (1989)
3. Munz, D., Yang, Y.Y.: Stress singularities at the interface in bonded dissimilar materials under mechanical and thermal loading. J. Appl. Mech. **59**, 857–861 (1992)
4. Munz, D., Fett, T., Yang, Y.Y.: The regular stress term in bonded dissimilar materials after a change in temperature. Eng. Fract. Mech. **44**(2), 185–194 (1993)
5. Qian, Z., Akisanya, A.R.: An experimental investigation of failure initiation in bonded joints. Acta Mater. **46**(14), 4895–4904 (1998)
6. Chen, D.H., Nonomura, K., Ushijima, K.: Stress intensity factor at the edge point of a bonded strip under thermal loading. JSME Int J. Ser. A **44**(4), 550–555 (2001)
7. Noda, N.A., Lan, X., Michinaka, K., Zhang, Y., Oda, K.: Stress intensity factor of an edge interface crack in a bonded semi-infinite plate. Trans. Jpn. Soc. Mech. Eng. Ser. A **76**(770), 1270–1277 (2010). (**in Japanese**)
8. Noda, N.-A., Lan, X.: Stress intensity factors for an edge interface crack in a bonded semi-infinite plate for arbitrary material combination. Int. J. Solids Struct. **49**, 1241–1251 (2012)
9. Mizuno, K., Miyazawa, K., Suga, T.: Characterization of thermal stress in ceramic/metal-joint. J. Fac. Eng. Univ. Tokyo (B) **39–4**, 401–412 (1988)
10. Ioka, S., Kubo, S., Ohji, K., Kishimoto, J.: Thermal residual stresses in bonded dissimilar materials and their singularity. JSME Int. J. Ser. A **39**(2), 197–203 (1996)
11. Erdogan, F.: Stress distribution in bonded dissimilar materials with cracks. J. Appl. Mech. **32**, 403–410 (1965)
12. Ikeda, T., Sun, C.T.: Stress intensity factor analysis for an interface crack between dissimilar isotropic materials under thermal stress. Int. J. Fract. **111**, 229–249 (2001)
13. Bogy, D.B.: Edge bonded dissimilar orthogonal elastic wedges under normal and shear loadings. J. Appl. Mech. **35**, 460–466 (1968)
14. Dundurs, J.: Effect of elastic constants on a stress in a composite under plane deformation. J. Compos. Mater. **1**, 310–322 (1967)
15. Oda, K., Noda, N.-A., Atluri, S.N.: Accurate determination of stress intensity factor for interface crack by finite element method. Key Eng. Mater. **353–358**, 3124–3127 (2007)
16. Kakuno, H., Oda, K., Morisaki, T.: Analysis of stress intensity factor for interfacial crack in bonded dissimilar plate under bending. Key Eng. Mater. **417–418**, 153–156 (2010)
17. Oda, K., Takahata, Y., Kasamura, Y., Noda, N.-A.: Stress intensity factor solution for edge interface crack based on the crack tip stress without the crack. Eng. Fract. Mech. (2019). https://doi.org/10.1016/j.engfracmech.2019.106612
18. Chen, D.H., Nisitani, H.: Singular stress field in jointed materials due to thermal residual stress. Trans. Jpn. Soc. Mech. Eng. Ser. A **59**(564), 1937–1941 (1993). (**in Japanese**)
19. Brown, E.J., Erdogan, F.: Thermal stresses in bonded materials containing cuts on the interface. Int. J. Eng. Sci. **6**(9), 517–529 (1968)